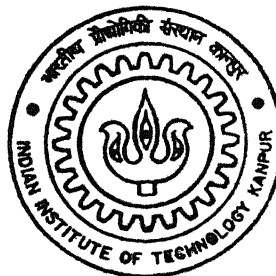# MIXING TIMES IN LADLES STIRRED WITH DUAL POROUS PLUG

By

Jayanta Mandal

DEPARTMENT OF MATERIALS & METALLURGICAL ENGINEERING

INDIAN·INSTITUTE OF TECHNOLOGY KANPUR

AUGUST, 2003

MIXING TIMES IN LADLES STIRRED

WITH DUAL POROUS PLUG

A Thesis Submitted

In Partial Fulfillment of the Requirements

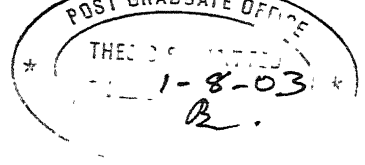*For the Degree of*

MASTER OF TECHNOLOGY

by

JAYANTA MANDAL

to the

DEPARTMENT OF MATERIALS AND METALLURGICAL ENGINEERING
INDIAN INSTITUTE OF TECHNOLOGY, KANPUR
AUGUST, 2003

CERTIFICATE

This is to certify that the present work **"MIXING TIMES IN LADLES STIRRED WITH DUAL POROUS PLUG"** has been carried out by Mr. Jayanta Mandal (Roll No. Y110608) towards his M.Tech. dissertation under my supervision and that this has not been submitted elsewhere for a degree.

(Prof. Dipak Mazumdar)
Department of Materials and Metallurgical Engineering
Indian Institute of Technology, Kanpur

August 1st, 2003

DR. DIPAK MAZUMDAR
Professor
Department of Materials
& Metallurgical Engineering
I.I.T. Kanpur-208 016

dedicated to …

my parents

ACKNOWLEDGEMENT

Foremost, I would like to express my sincere gratitude to my respected guide Dr. Dipak Mazumdar for his kind guidance and invaluable suggestions that have helped this thesis-work to assume a meaningful shape. I am grateful to him for providing me with useful references, materials and books that enriched my knowledge and understanding about the problem in hand. A lot many thanks too for giving me full freedom to think and approach in my own way and finally for carefully editing this report. Without his cooperation, it would not have been possible for me to complete this thesis work in time. I am also thankful to him for his precious advices in my personal life.

In the course of my thesis work, a number of other persons, too, stretched their helpful hands to me, whenever I was in need. Discussions with Satish, Madan and Surendra were always fruitful; it helped me solving a number of critical problems. I am also thankful to SharmaJi and all the technical stuff of the department for their direct and indirect assistance towards the project.

It will be very difficult for me to forget the happy, interesting moments with Debi, Gopi, Kausik, Debasish, Bikas, Debu, Shila, PinakiDa, DebdasDa, RajibDa and last but not the least KausikDa, who made my IITK-life memorable during my stay over here.

Finally, I sincerely owe to my parents and my sister. Their continuous encouragement, support, blessing, guidance have brought me to the portals of my present achievement.

Jayanta Mandal

ABSTRACT

Mixing times in three different cylindrical shaped vessels (viz. Diameter =0.60m, 0.45m and 0.30m respectively) and a 0.194 scale tapered vessel (Bottom Diameter = 0.52m, Top Diameter = 0.58m and Angle of Taper = 2.34°) in which, water was stirred by injecting air/N_2 through two diametrically opposite nozzle were investigated via the electrical conductivity measurement technique following the addition of pulse tracer to the bath. Regression analysis of the experimental data indicated that dimensionless, 95% bulk mixing times, $\tau_{mix, 95\%}$ can be correlated with the key operating variables, L (the depth of the liquid in the vessel), R (the radius of the vessel) and the ambient gas flow rate Q (referenced to the mean height and temperature of the bath) according to:

$$\tau_{mix, 95\%} \approx 23.9 \, Q^{-0.27} \, L^{-0.47} \, R^{1.65} \qquad \text{for plugs located at } \tfrac{1}{3}R \text{ positions}$$

$$\text{And} \quad \tau_{mix, 95\%} \approx 23.4 \, Q^{-0.28} \, L^{-0.52} \, R^{1.72} \qquad \text{for plugs located at } \tfrac{1}{2}R \text{ positions}$$

It was confirmed experimentally that in the inertial force dominated flow regime twin nozzles with equal net gas flows leads to somewhat shorter mixing times than those observed in an equivalent system stirred with axisymmetrically placed single plug However, for the twin plug stirred system, not much influence of plug locations on measured mixing times was observed. Within the range of parameters investigated both ½R as well as ⅓R positions of the plug were found to lead to practically similar mixing times.

Two cases were being studied in case of the tapered vessel. In one case, experiments were carried for a constant liquid volume as that in cylindrical vessel where as in the other, the L/D ratios were kept constant as that of the cylindrical vessel. It was found out that mixing times in the tapered vessel could also be favorably described via the correlation derived in the present work from cylindrical shaped ladles.

TABLE OF CONTENTS

CHAPTER 1

INTRODUCTION

CHAPTER 2

EXPERIMENTAL WORK

CHAPTER 3

RESULTS AND DISCUSSION

CHAPTER 4
CONCLUSIONS

CHAPTER 5
RECOMMENDATIONS FOR FUTURE WORK

BIBLIOGRAPHY

APPENDIX

LIST OF SYMBOLS

a : Dimensionless constant related to geometric aspect ratio, L/R

b : Dimensionless constant related to dimensionless gas flow rate, Q^2/gR^5

C_0 : The dimensionless pre-exponent, is a function of the mode of gas injection (symmetrical or asymmetrical), the degree of mixing, the location of tracer injection, the monitoring point, etc.

D : Diameter of vessel, in metre

D_{eff} : Effective diameter of tapered vessel, in metre

E : Rate of energy input per unit volume of liquid

E_b : Rate of buoyancy or potential energy input per unit volume of liquid

E_k : Rate of kinetic energy input per unit volume of liquid

g : Acceleration due to gravity ($= 9.81 m/s^2$)

H : Notation used for bath depth in tapered vessel (Equation 3.7)

L : Bath depth, in metre

L_m : Depth of liquid in the model, in metre

L_{fs} : Depth of liquid in the full scale ladle, in metre

M : Mean of the sample

N : Number of scores

Q : Gas flow rate corrected with reference to operating temperature (1600°C) and mean hydrostatic pressure i.e. the hydrostatic pressure at mid bath depth.

Q_m : Gas flow rate in model, in m^3/s

Q_{fs} : Gas flow rate in the industrial full scale ladle, in m^3/s

Q_{sp} : Specific gas flow rate, in $m^3/min.ton$

R : Vessel radius, in metre

R_m : Radius of model vessel, in metre

R_{fs} : Radius of the prototype, in metre

R_0 : Radius of the vessel at a particular liquid depth, in metre

R_B : Base radius of the tapered vessel (=0.26m)

R_{eff} : Effective radius of the tapered vessel defined as half of the summation of base radius and radius at surface corresponding to bath depth, in metre

τ_{mix} : Experimental mixing time, in sec

$\tau_{mix,\,95\%}$: 95% bulk mixing time, in sec

$\tau_{mix,\,m}$: Mixing time in model, in s

$\tau_{mix,\,fs}$: Mixing time in full scale ladle, in s

θ : Angle corresponding to the nozzles located at base of the vessel

β : Fractional depth of lance submergence (see Figure 1.16)

λ : Geometrical scale factor defined by the ratio of diameter of the model to the diameter of full scale ladle system

ϕ : Notation used to denote diameter of vessel.

Π : Raleigh's notation for dimensionless number/group

π : PI (= 3.141592654)

ρ_{Steel} : Density of steel (= 7000 kg/m^3)

σ_{rms} : Root-mean-square deviation

S^2 : A biased estimation of variance

σ^2 : Variance

μ : Mean

LIST OF FIGURES

LIST OF TABLES

CHAPTER 1

INTRODUCTION

1.1   INTRODUCTION TO THE THESIS

In the last few decades there has been a considerable effort in improving and developing new processes for the post steelmaking refining of steel. It is very difficult to carry out certain aspects of refining in oxidizing conditions in an oxygen steelmaking furnace or in an electric furnace. For example, desulphurization is best carried out under reducing conditions when oxygen content of the steel is very low. In addition, by carrying out such operations outside the steel making furnaces, valuable furnace time and steelmaking fluxes are saved [1].

In steelmaking, gas injection is applied on routine basis, at various stages of melt refining, to enhance reaction rates, eliminate thermal and/or composition gradients, to remove particulate and so on [2]. Secondary refining or ladle process embodying N_2 or Ar gas injection has grown dramatically in the past few years due to the need for cleaner steels and higher productivity. A ladle process can be used for the purpose of inclusion removal, desulphurization, dephosporization, and alloying. The advantage of ladle refining process by gas injection are that its capital cost is low, it homogenizes the bath, enhances inclusion flotation, and provides good refining efficiency owing to a faster approach to equilibrium because of better mass transfer rate between metal and slag or gas [3, 4]. In a gas stirred ladle, bubbles rising through the liquid induce a recirculatory flow of fluid because of the reduced density in a gas /liquid plume. As a disadvantage, this process exposes the liquid steel to the atmosphere, resulting nitrogen pickup and reoxidation of steel.

1

In the early days of steelmaking ladles were originally designed for transporting molten iron from the iron blast furnace to steel making vessels, and from there to ingot pouring bays. Now-a-days it is not only used as a transporting medium but at the same time it is used as a refining reservoir. Gas is purged through the bottom tuyere/nozzle or by lancing from the top and unit operations like deoxidation, dephosporisation, desulphurization, alloying addition, inclusion float out are carried out in such systems to make cleaner and superior quality of steel. By doing all these chemical operations inside a ladle, the cost of production of steel can be reduced as it interns saves valuable furnace time and flux consumption. Therefore, the role of ladles has enlarged in recent years to include in transit chemical and physical processing operations. Thus, one can now identify three main areas where ladle metallurgy has provided new possibilities [5].

1. **Chemistry:** By the removal of unwanted elements, (S, Si, P, O, C, H, N) from iron and steel, new grades are possible and overall product quality is improved.

2. **Control:** It allows close quality control of physical and chemical characteristics to be achieved (i.e. Inclusion type, size and amount, dissolved gas content, etc.).

3. **Productivity:** The main functions of the primary processing vessels are to provide 'raw' iron or steel. They are not interrupted by any secondary refining operations carried out in transfer vessels or ladles.

In Figure 1.1 a schematic of gas purging in a filled ladle of steel is shown. The shell of a ladle is welded of sheet steel in the form of a truncated cone with a spherical bottom [6]. The volume of a ladle is calculated so as to accommodate the whole mass of the tapped metal and a certain (5-10%) layer of slag. Various refining operations like deoxidation, dephosporisation, desulphurization are carried out by purging N_2 or Ar into the molten metal bath through bottom nozzle. Teeming ladles are lined with fireclay, magnesite-dolomite or high alumina refractories. The lining may be either bricklaid or monolithic. The lining is worn unevenly, the greatest wear being observed in places where the metal jet strikes the lining and in the slag belt region. The teeming arrangement of a ladle comprises a stopper and a casting nozzle. The casting nozzle is mounted in a hole provided in the ladle bottom. Vertical stopper that pass in the ladle vertically through the whole mass of the metal (see Figure 1.1). The stopper can be lifted and lowered by a lever

2

mechanism. Upon lifting, the lower end of the stopper opens the nozzle and metal is allowed to flow in the next section i.e. in tundish. The stopper comprises a solid or hollow metallic rod onto which a number of fireclay sleeves are inserted.
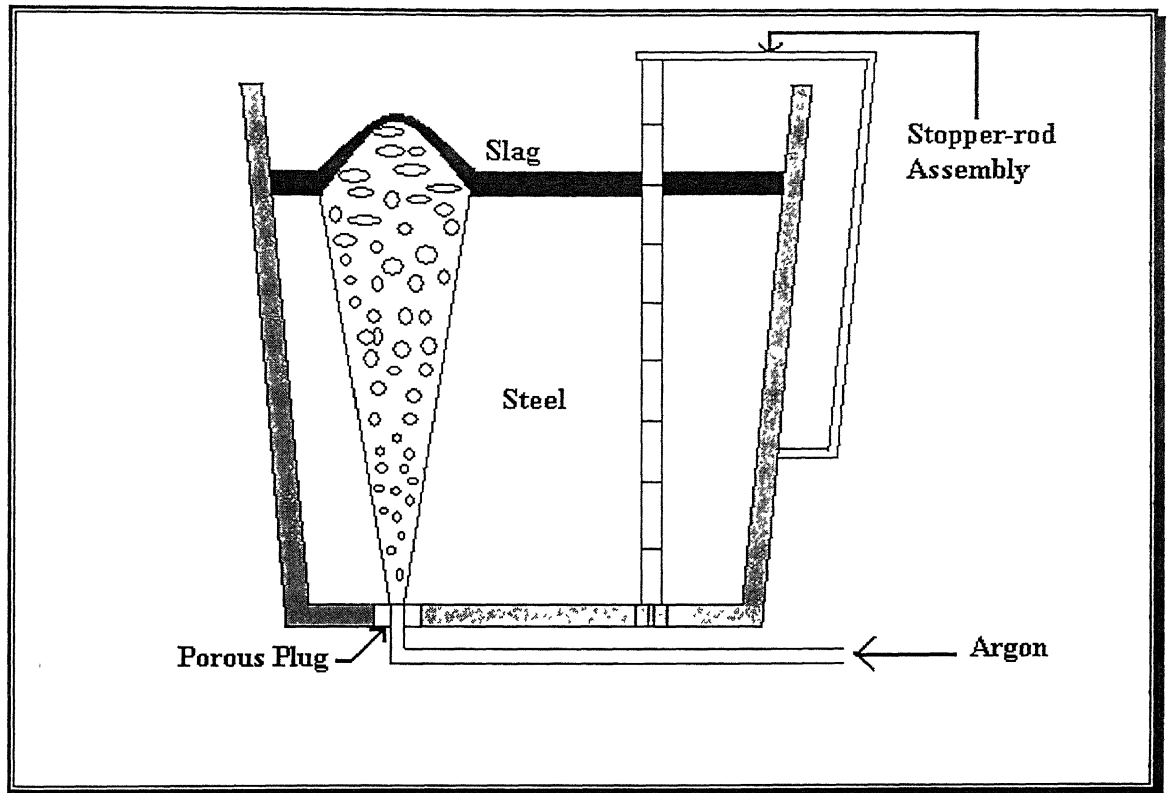
Figure 1.1: Schematic of gas purging in a filled ladle of steel.

When an inert gas is injected into ladle containing molten steel from the bottom at a moderate flow rate, it comes out of the nozzle/porous plug/lance and rises in the form of discrete gas bubbles. The gas bubbles rise to bath surface due to buoyancy and because of this good agitation/circulation induces in the bath. The characteristics of the induced flow, (see Figure 1.1) which is invariably turbulent in nature, influences the rate of numerous processes such as dissolution/melting, dispersion, slag metal reaction etc. and thus plays a decisive role in the overall process performance of the gas stirred ladle systems. As a disadvantage, this process exposes the liquid steel to the atmosphere, resulting nitrogen pickup and reoxidation of steel. So, in principle it is suggested to carry out the refining

reaction in the ladle under low flow rates or at times under an inert atmosphere such that quality steel can be produced. While typically, under industrial conditions, only relatively low gas flow rates are applied to achieve thermal and/or chemical homogenization, somewhat intense stirring condition can also be practiced for accelerating slag-metal reactions [2].

Gas-stirring of steel in ladles is applied on a routine basis, at various stages of melt refining to achieve certain objectives. The objectives of the stirring process are the following [1]:

1. Alloy addition and control of final chemistry.
2. Improved deoxidation.
3. Improved temperature and composition homogenization.
4. Inclusion floating.
5. Desulphurization.
6. Sulphide shape control.
7. Oxide shape control.
8. Vacuum degassing of hydrogen.
9. Dephosphorisation.

Further development will also be concerned with the removal of nitrogen and tramp elements.

1.2   LITERATURE REVIEW ON MIXING PHENOMENA

The mixing phenomenon in metallurgical systems containing molten metal has been normally characterized by "mixing time" [7]. The mixing time is defined as the time required to attend a desired level of homogeneity in the bath or desired value of degree of mixing [8]. MacDonald [9] defined the mixing time as the time required for a slug of feed solution to be dispersed homogeneously throughout the vessel in a batch operation or in a continuous flow system. With low intensities of agitation the mixing time will be large,

4

while increasing the intensity will results in decreasing the mixing time. It is generally believed that the mixing is more effective when the gas is injected from the bottom of the vessel [10, 11, 12]. When the gas is injected into a liquid bath from the bottom at a moderate flow rate it comes out of the nozzle in the form of gas bubbles. These gas bubbles rise to the bath due to buoyancy effect and impart momentum to the surrounding liquid, causing gross circulation in the bath and thereby promoting mixing. It is also interesting to note that tapering in the vessel causes a secondary recirculatory motion in the bottom outside corner of a typical ladle as shown in Figure 1.2 [5, 13]. Mazumdar [14] observed that mixing time depends on the points of tracer injection and monitoring. He further demonstrated that the mixing in the gas injection ladles can be expected to be controlled by a combination of eddy diffusion and bulk convection, both mechanisms contributing in roughly equal proportions.
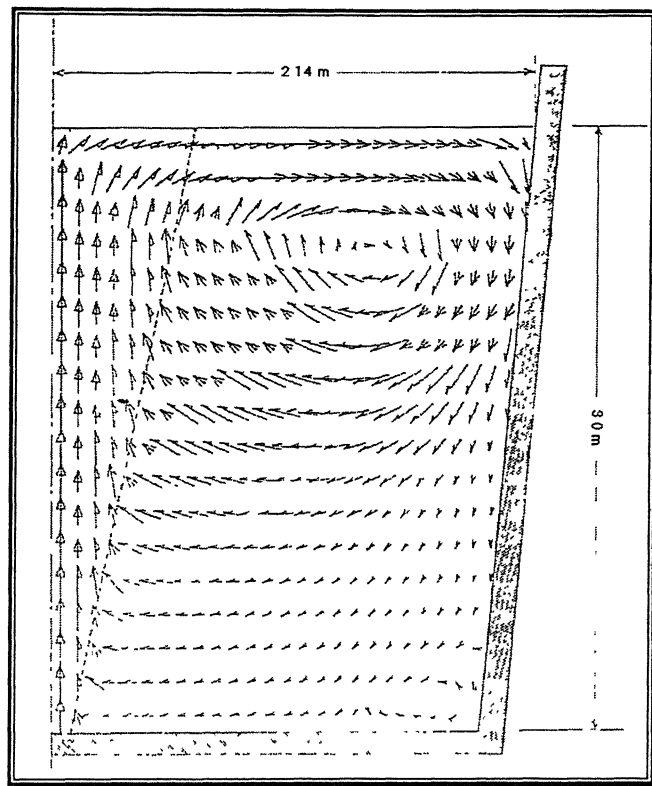
Figure 1.2: Predicted velocity field in a 250 ton ladle of steel with central gas injection at 0.25 Nm^3min^{-1}.

1.2.1 Various Types of Measurement Techniques

Many studies have been carried out on the determination of mixing times in water models of gas stirred ladles. These studies have used different types of measurement techniques to investigate a wide variety of gas injection configurations. These are described below in brief. Although it is desirable to measure the mixing time directly in high temperature melts, it is expensive and difficult. To overcome this problem, cold water model studies are often carried out. One of the most commonly used techniques of measuring mixing time is "stimulus response technique". Based on this various methods of measuring mixing time in liquid bath at room temperature (i.e. isothermal condition is maintained during the entire processing operation) have been developed and reported. These include color dye technique [9, 15], decolorization technique [16, 17], measurement of temperature profile using thermocouples [16, 18], refractive index measurement [19], pH measurement [20, 21], and electrical conductivity measurement [8, 22, 23].

1.2.1.1   Color dye technique

To follow the mixing time visually throughout the vessel this method is adopted. Addition of a die to a clear liquid renders it possible to follow the initial stages very clearly. However, in the final stages, nearly the whole vessel contents are colored and further changes are then difficult to see [15]. This is a crude method of measuring mixing and therefore liable to contain significant error.

1.2.1.2   Decolorization technique

This method is well adopted to overcome the difficulties observed in color dye technique at the final stages of operation. In this case the experiment is started with a color batch of liquid, which gradually clears as mixing proceeds in presence of an indicator (also acts as a tracer), stagnant zones appearing as colored patches while the bulk is already clear [16]. There are, however, parts of the liquid near stationary vessel walls that are often not

decolorized and neglected. Koria and Lange [17] use a 0.05 mole/l iodine solution in addition to a 0.5-1% starch solution to color the bath. A 2 mole/l sodium thiosulphate solution is used as a tracer liquid to decolorize the bath. At low flow rates of the injecting gas, some stagnant zones appearing as colored patches were observed due to non-uniform decolorization. On the other hand, decolourization occurs relatively more uniformly over the entire liquid volume and no stagnant zones have been observed when the flow rates were high. Accurate estimation of mixing times is however not feasible through such technique.

1.2.1.3   Temperature measurement technique

In this method a small amount (1-2%) of heated (20-40°C) liquid is added to the bath and the temperature is measured using thermocouples located at several positions in the vessel to monitor homogenization. This yields quantitative information on the progress of mixing at these locations. An advantage of the thermal method is that for the positions measured it gives a uniquely defined quantitative mixing time [18].

1.2.1.4   Refractive index measurement technique

In this mixing is determined by "Schlieren" method [19]. Optical inhomogeneities in the liquid in the vessel, in the form of gradients in refractive indices, produce "Schlieren". Absence of the "Schlieren" indicates homogeneity of the bulk liquid. In order to avoid refraction, the cylindrical vessel is placed within a vessel, with plane-parallel walls.

The starting point of the experiment is taken at a point in which the two liquids formed superimposed layers of fluids. If the liquids are carefully introduced into the vessel the interface is clearly visible. The mixing time is the time elapsed between the moment the stirring is started and the moment of disappearance of the "Schlieren". It should be noted that the difference in refractive index has no influence on the time required to

homogenize the two liquids i.e. the mixing time. Measurements made at a given difference in density give the same mixing time irrespective of the difference in refractive index. Experiments have shown, however, that the intensity of the "Schlieren" is influenced only by the difference in refractive index [19].

1.2.1.5 pH measurement technique

In pH method, a tracer in the form of acid, alkali or a salt solution is injected as an impulse and variation in pH as a function of time is recorded [20]. Sinha and McNallan [21] used 75% H_2SO_4 as a tracer solution and add approximately 3 ml of tracer for each experiment. The added of tracer contains sufficient H^+ ion to reduce the pH of water to 3, and mixing is considered to be complete when the pH of the solution has stabilized to within ± 0.01 pH units. However, pH measurement suffers some limitations, which are [8]:

(i)   pH probe is fragile and therefore difficult to handle, and

(ii)   pH of the bath is proportional to the logarithm of the tracer concentration that shows less sensitivity to concentration variations during mixing.

Position of tracer addition has significant influence on mixing time [21]. The locations near the top of the bath give much more rapid mixing than the locations near the bottom of the bath. Guthrie and co-workers [24, 25, 26] explained that this is because of high turbulent mixing/eddy diffusion viscosity near the top of the bath. Tracer added in the region of high turbulent viscosity results in shorter mixing time because of high eddy diffusivity. On the other hand, when tracer is injected in relatively slow moving region the mixing time is expected to correspondingly higher. When the system is very near to equilibrium (viz. complete homogenisation), the last stage of solute redistribution into poorly mixed regions of the bath may occur primarily by molecular diffusion rather than turbulent diffusion, which is rather slow process.

1.2.1.6 Electrical conductivity measurement technique

Of the various methods reported in the literature for the measurement of mixing time, electrical conductivity measurement technique is perhaps the best [8]. Acid, alkali or salt solution is added as a pulse tracer and change in electrical conductivity recorded against time elapsed. Both pH and electrical conductivity measurement techniques are very similar in measurement techniques, but the later have some unique advantage over the former. The electrical conductivity probe is sturdy and has faster response. Moreover, electrical conductivity varies linearly with the tracer concentration [22]. The electrical conductivity probe can be used for a wide range of homogenization measurements and thus one can easily estimate the precise value of mixing time.

During a typical measurement, air is injected into the water bath through the nozzle(s) located at the bottom of the vessel at a specified flow rate for 10 to 15 minutes to ensure the stability of flow in the vessel as well as to homogenize the initial bath composition. On addition of KCl solution [8] as a tracer, considerable oscillations in the form of peaks and valleys are recorded via conductivity probe. These peaks and valleys results from the concentration fluctuations at the probe tip arising from inhomogeneities of the tracer concentration in the bath. The fluctuations gradually diminish as the time progress and attain a steady value that is reflected as an almost steady voltage output from the probe [23]. From such mixing times can be determined fairly accurately.

1.2.2 Gas Injection Configuration

Mixing times in gas stirred vessels have been determined experimentally under a wide variety of gas injection configurations. Essentially, in cylindrical shaped vessels, gas is injected through one or more nozzles located asymmetrically or symmetrically at the base of the vessel. A schematic of the various configurations studied are shown in Figure 1.3. Some experiments were carried out for these configurations using a simulated slag as well.
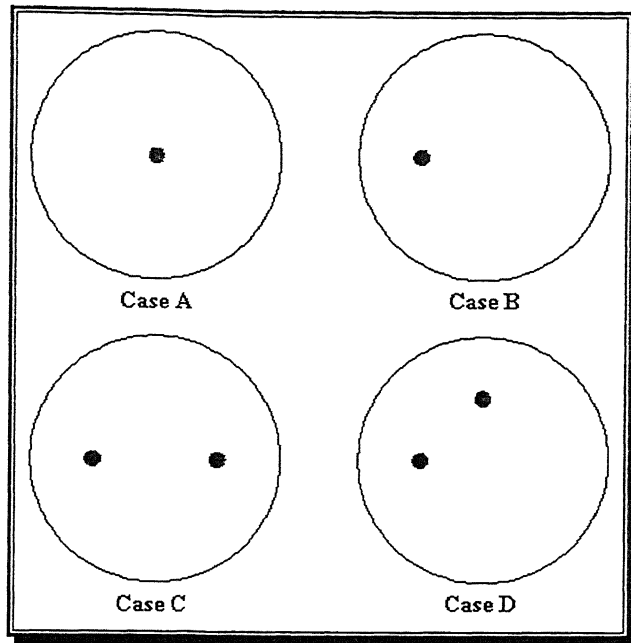
Figure 1.3: Nozzle configurations used form experimental study in model ladle.

1.2.2.1 Mixing in axisymmetrical single plug gas injection configuration

Figure 1.4 (a) and (b) show the predicted flow pattern at the main vertical plane (the plane passes through the axis of the cylindrical vessel) and at the top horizontal plane (free surface) respectively (Case A). It can be seen that two axisymmetric recirculations are formed in the bath and the velocity in the plume zone and near the sidewalls and free surface are relatively large. However, owing to symmetry, there is no angular velocity in this case of axisymmetric flow [27].

Mixing in case of axisymmetric single plug is sensitive to the position of tracer addition, as there is almost no angular mixing in the ladle. Figure 1.5 shows the predicted and measured value of mixing time in the ladle with various arrangements of nozzle(s) for three different tracer adding positions.

10

(a) **(b)**
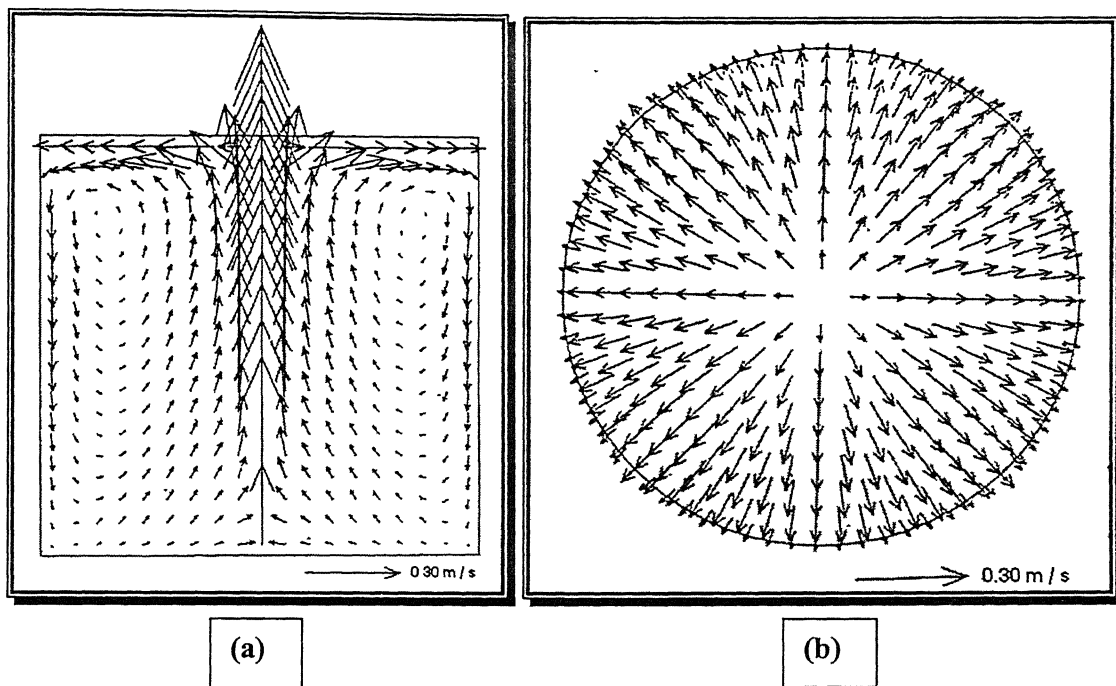
Figure 1.4: (a) Predicted flow pattern as single nozzle is placed at center in the ladle (Case A, argon flow rate 6 Nl/min).

(b) Predicted flow pattern at free surface in the ladle (Case A, argon flow rate 6 Nl/min).
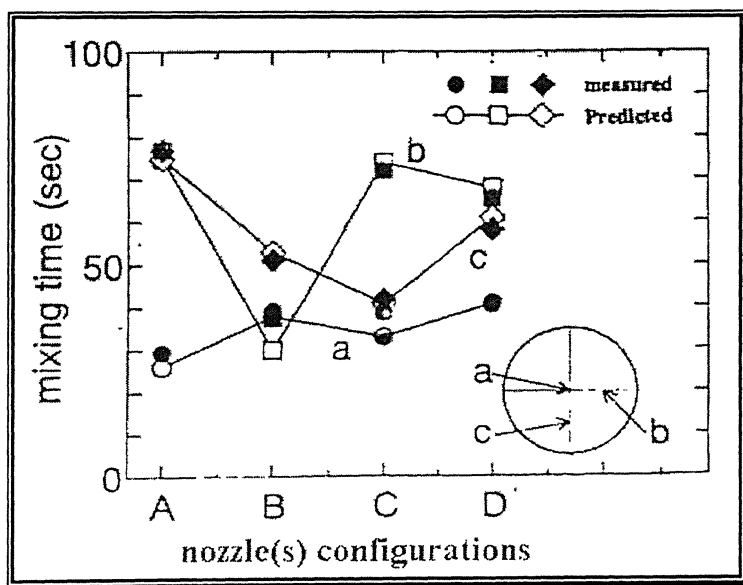
Figure 1.5: Predicted and measured mixing time for each tracer adding position at different nozzle(s) configurations (gas flow rate 6 Nl/min).

11

1.2.2.2 Mixing in asymmetrical single plug gas injection configuration

Figures 1.6 (a) and (b) show the predicted flow pattern at the main vertical plane and at the top horizontal plane (free surface) respectively (Case B) when argon gas is injected through the nozzle [27]. In Case B the nozzle is located not at the centre but at R/2 (mid radius) position. In this case, in contrast with axisymmetric bubbling, the velocity in the plume zone and near the side wall decreases. However, the angular velocity has a great effect on the mixing in the ladle and the velocity near the bottom increases significantly.

Addition of tracer at various locations does not have much influence on mixing in case of asymmetric plug location due to large angular velocity. This is clearly reflected in Figure 1.5.

Figure 1.7 shows that mixing time decreases according ~1/3 power to gas flow rate for various bubbler locations. On the other hand, Figure 1.8 shows mixing time for the radial position for a single nozzle for different gas flow rate. It can be concluded from the above figure that single nozzle located at half radius position will results in better bulk mixing and consequently would lead generates minimum mixing time. As one moves away from the center toward half radius position for the plug, mixing time decreases, giving minimum mixing time at half radius position of the plug and then again increases as one moves toward the wall of the vessel [28].

(a)

(b)
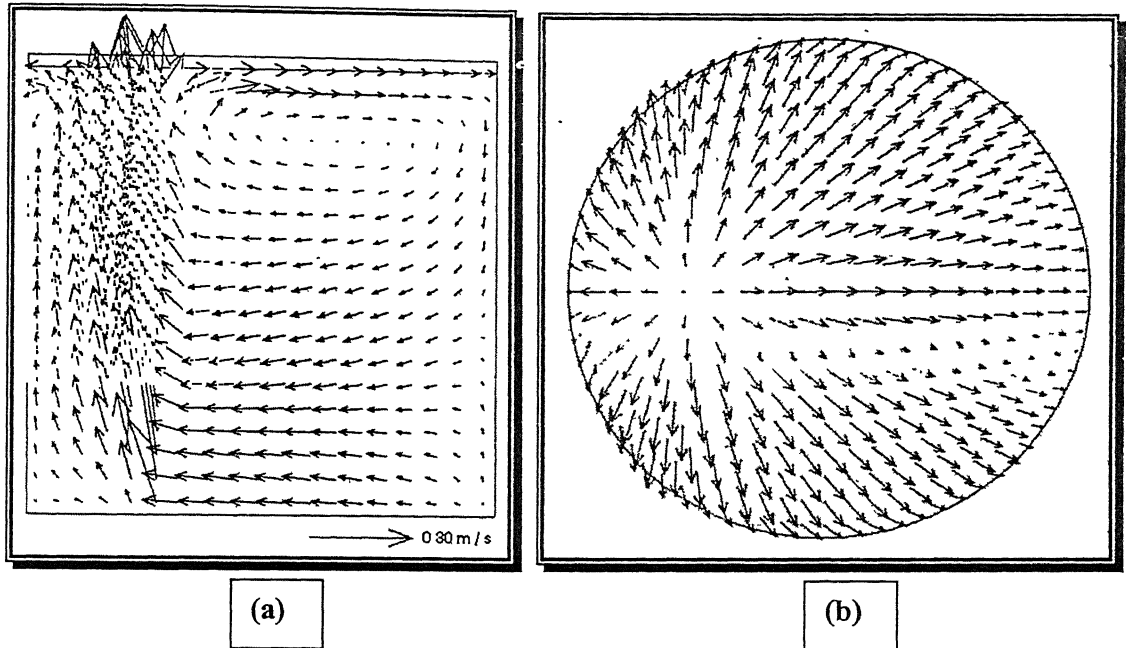
Figure 1.6: (a) Predicted flow pattern as single nozzle is placed at half radius in the ladle (Case B, argon flow rate 6 Nl/min).

(b) Predicted flow pattern at free surface in the ladle (Case B, argon flow rate 6 Nl/min).
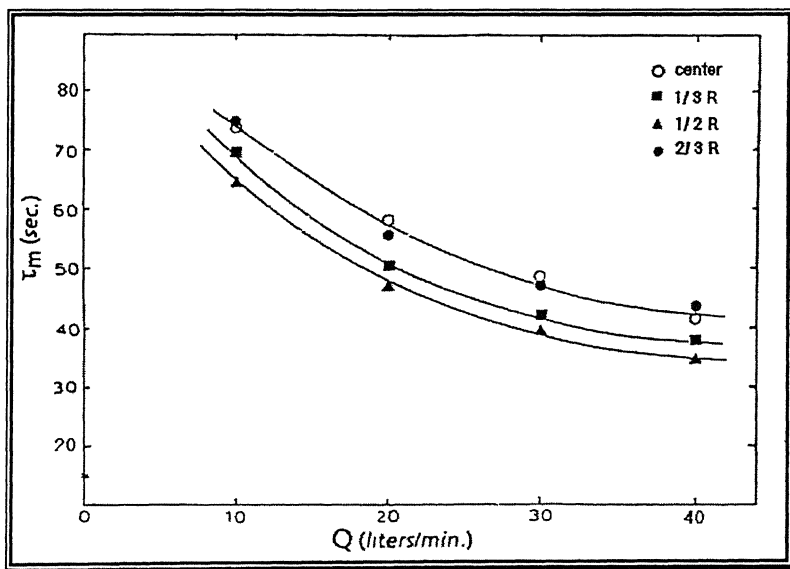
Figure 1.7: Variation in 95% mixing times with gas flow rate for plug placed at center, one-third, half and two-third radius of ladle base.
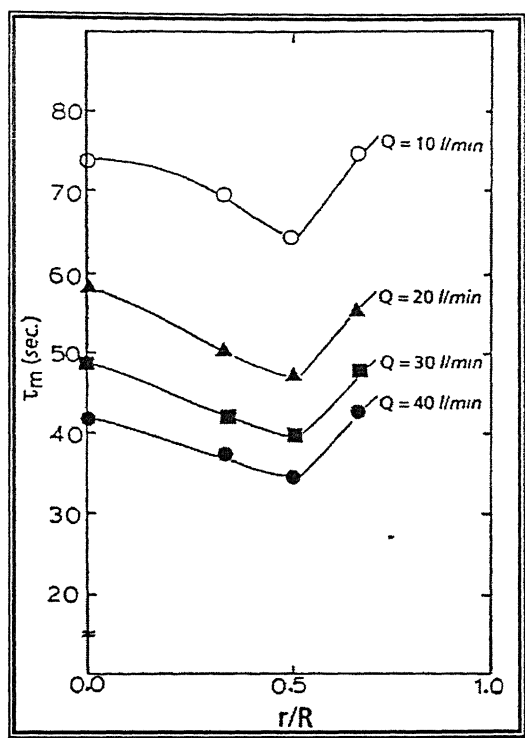
Figure 1.8: A plot of mixing time vs. radial position for a single plug for various flow rates.

1.2.2.3 Mixing in dual plug gas injection configuration

Figures 1.9 (a) and (b) show the predicted and visualized flow patterns at the central vertical plane i.e., the plane passing through the axis of the vessel containing both the nozzles and at the free surface (Case C) whereas Figure 1.10 (a) and (b) show the predicted and visualized flow patterns at the vertical plane joins the centre and one nozzle and at the top horizontal plane i.e., at the free surface (Case D) respectively. Figure 1.9 (a) shows the fluid movement is in upwards direction and recirculates in the region of top surface. It is to be noted here that there is no dead zone in Case C when two nozzles are placed diametrically opposite at half radii position. On the other hand, Figure 1.10 (a) shows (Case D) that the fluid movement is in downwards direction near the side walls. The total average velocity seemed to be smaller in this case and there is a dead zone at the corner between the side and the bottom wall. It appears that velocity field is more homogeneous in Case C than

in Case D, which implies good mixing in the ladle. This also include that Case C is less prone to splashing, spitting and non-metallic inclusion entrapment into the molten steel [27].

As mentioned earlier that addition of tracer at various locations does not have any significant influence on mixing in case of asymmetric plug location due to large angular velocity. Thus mixing time becomes insensitive to the tracer adding position in case of either Case C or Case D.

(a) (b)
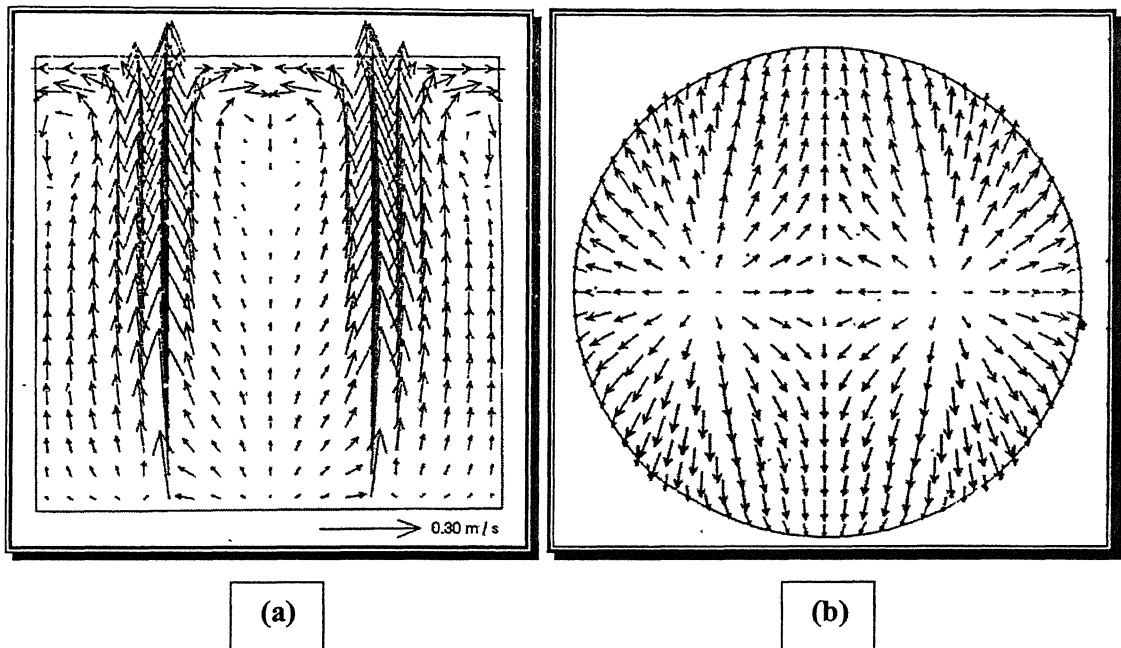
Figure 1.9: (a) Predicted flow pattern as two nozzles are opposite place at half radii in the ladle (Case C, argon flow rate 6 Nl/min).
(b) Predicted flow pattern at free surface in the ladle (Case C, argon flow rate 6 Nl/min).

(a)   **(b)**
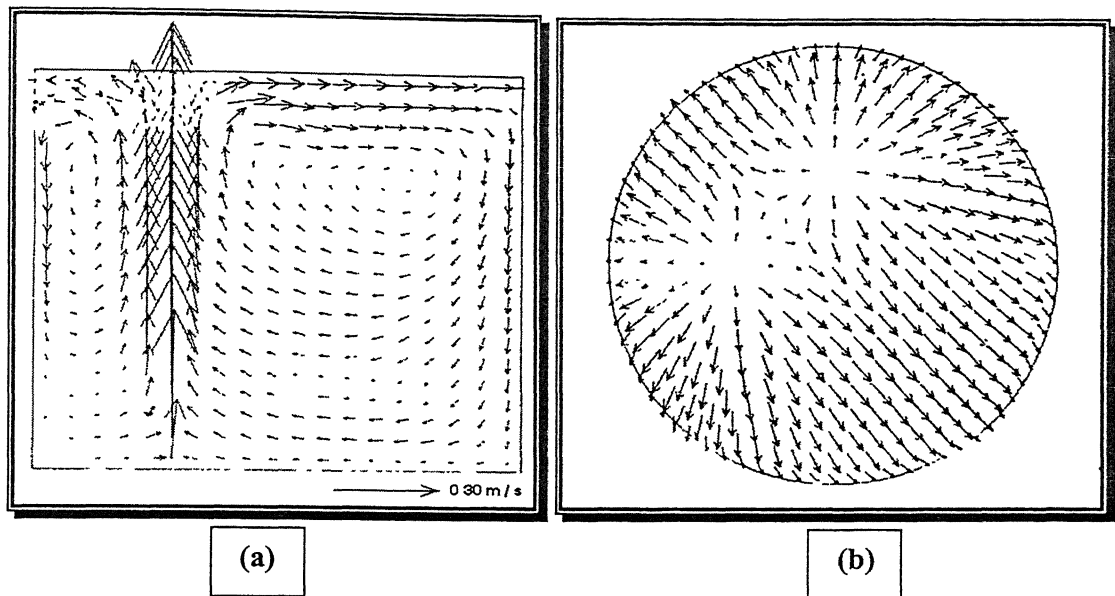
Figure 1.10: (a) Predicted flow pattern as two nozzles are vertically placed at half radii in the ladle (Case D, argon flow rate 6 Nl/min).

(b) Predicted flow pattern at free surface in the ladle (Case D, argon flow rate 6 Nl/min).

Figure 1.11 shows the effects of two gas injection nozzles at the bottom of the vessel for various plug locations [28]. There experimental mixing times are plotted vs. net flow rate of gas. One nozzle is located at various location such as $\theta = \pi/4$, $\pi/2$, $3\pi/4$ and π with other nozzle at $\theta = 0$ position. Out of all the combinations, minimum mixing time results when the two nozzles are placed at midradius and diametrically opposite to each other ($\theta = 0$ and π respectively).

Figure 1.12 shows mixing time against gas flow rate when two plugs are located at diametrically opposite to each other but at (1/3)R, (1/2)R and (2/3)R positions respectively. It is seen from the above figure that mixing time is minimum for two nozzles located at half radii.
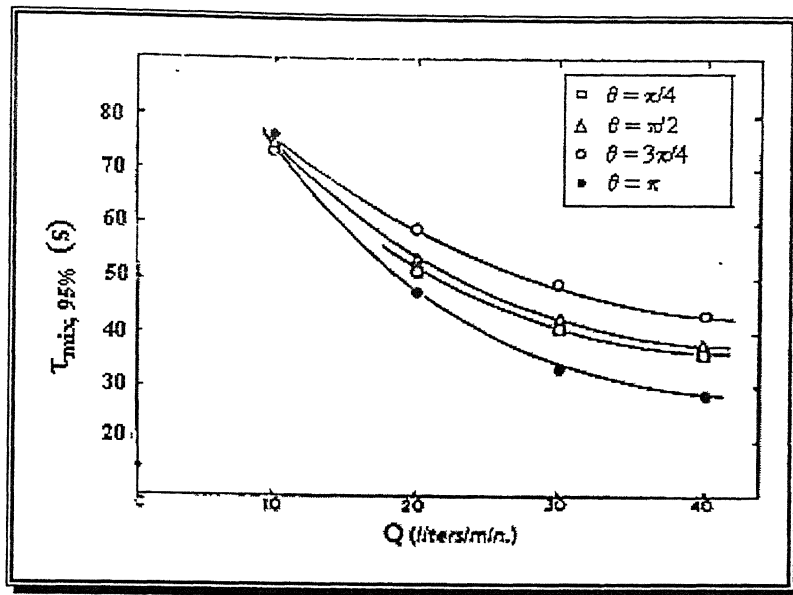
Figure 1.11: Variation in 95% mixing times with gas flow rate for double plug arrangements, placed at midradius. The effect of angle, θ, subtended between the two plugs, is illustrated.
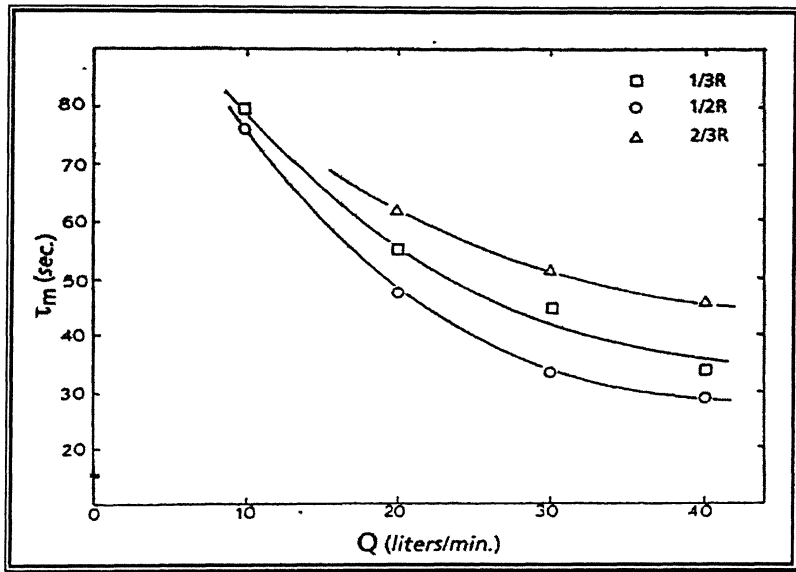
Figure 1.12: Variation in 95% mixing times with symmetrical changes in the radial positions of the two opposing plugs ($\theta = 180^0$).

17

1.2.3 Effect of Mixing Time in Presence of a Slag Phase

Figure 1.13 shows a plot of mixing time as a function of gas flow rate for center, an off center, and a side nozzle with an overlaying oil layer. A 50/50 mixture (by volume) of paraffin oil and cottonseed oil is used as a slag phase in cold model study [4]. Similarly, Figure 1.14 shows a plot of mixing time in terms of stirring energy density. It is seen that, in presence of an oil layer, mixing times is significantly longer regardless of injection pattern. In presence of the oil layer, some of the stirring energy by the gas injection through the bottom of the vessel is consumed in producing turbulence at the interfacial region and a circulation inside the oil. Therefore, less energy is used for the mixing phenomena to occur inside the bulk phase. This effect implies the resistance of an oil layer to the recirculatory velocity of bulk fluid.
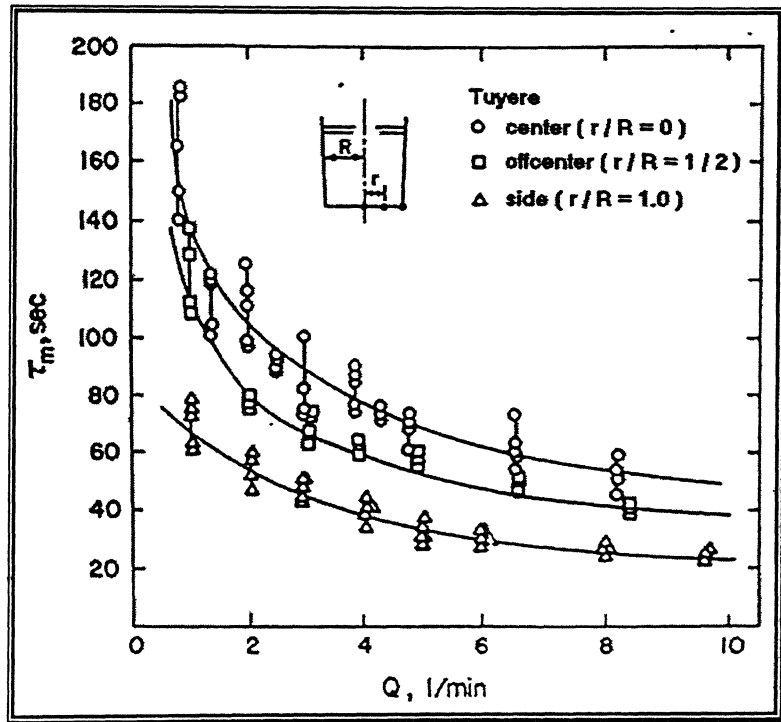
Figure1.13: A plot of mixing time as a function gas flow rate for three different arrangement of nozzle with an oil layer present
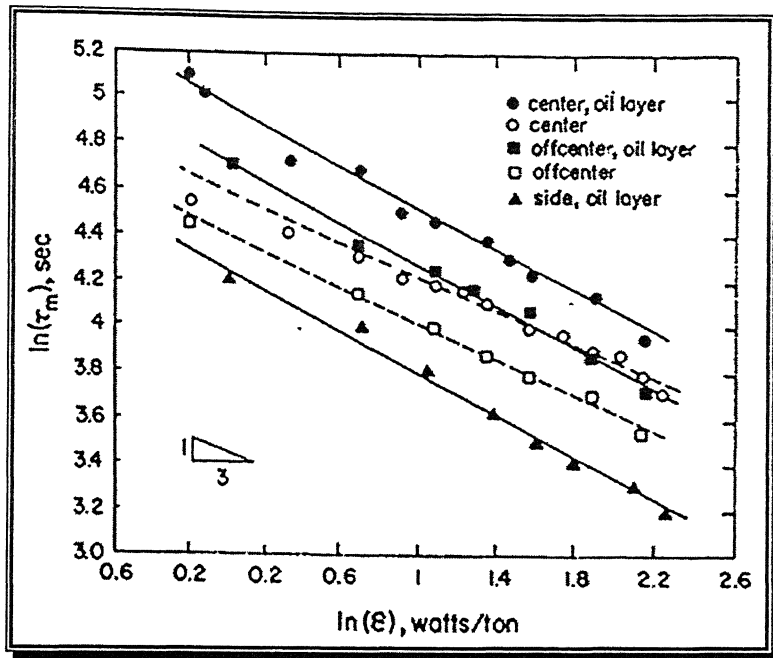
Figure 1.14: Mixing time vs. stirring energy density for three different nozzle patterns with and without oil layer.

1.2.4 Influence of Monitoring Points on Mixing Time

Several investigators [21, 28, 29, 30, 31] have reported that the state of mixing in a gas stirred bath under a given set of operating conditions is a function both tracer addition point as well as the monitoring point locations. In Figure 1.15 it is shown that the probe location as well as tracer addition point in combination appears to have significant effects on measured mixing time at various locations in the vessel. This phenomenon was observed at low gas flow rates (e.g., in the range applied to typical ladle gas injection operations). However, at large values of specific gas flow rate applied in a relatively small vessel, the state of mixing in most parts of the reactor is relatively uniform.
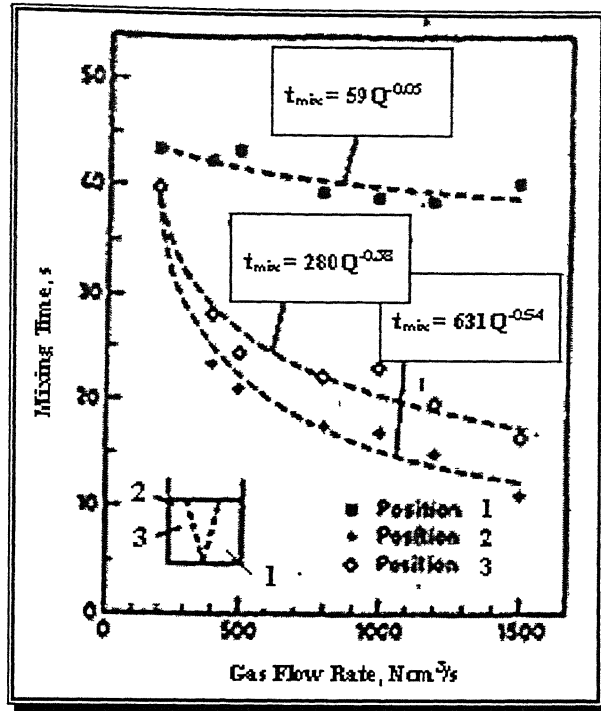
Figure 1.15: Influence of monitoring point location on the measured mixing times for central nozzle position and tracer addition in the dead zone.

1.2.5 Influence of Operating Variables on Mixing Time

The change in predicted mixing time with the change in injected gas flow rate for all the cases mentioned above (viz. Case A, Case B, Case C, Case D) is shown in Figure 1.5. In general, we can say that the mixing time decreases with increasing gas flow rate. Mazumdar and Guthrie [31] and numerous other investigators determined experimentally that mixing time is proportional to $Q^{-1/3}$. At low gas flow rate the relationship changes to $Q^{-0.48}$ Figure 1.16 shows how mixing time changes with gas flow rate for an aqueous model of a gas stirred ladle.
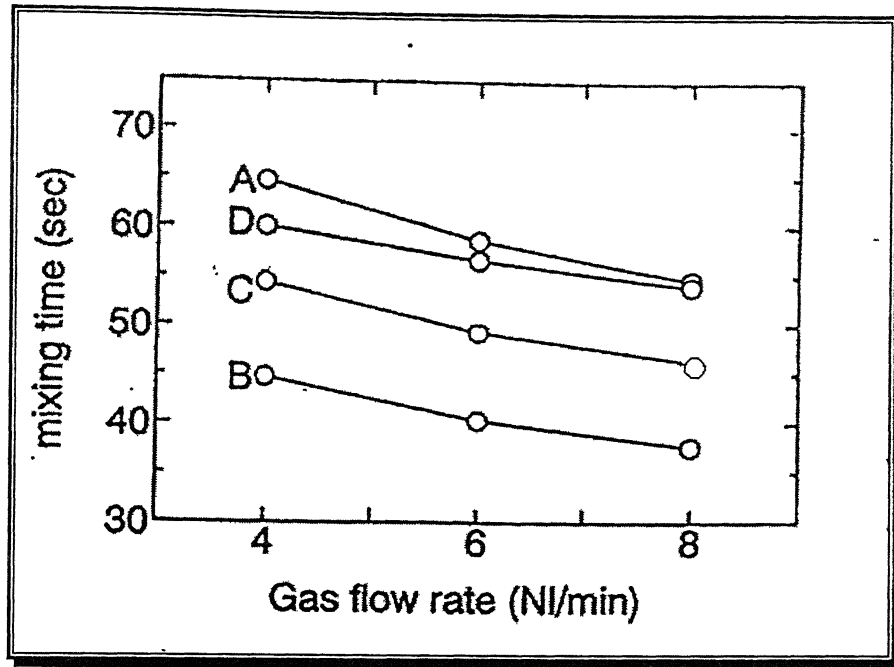
Figure 1.16: Effect of gas flow rate with mixing time for different nozzle(s) configurations.

When the gas (N_2 / Argon) is injected through the bottom of the vessel, it provides required energy for the mixing of the bath. The rate of energy input E is theoretically equal to the rate of input of kinetic energy (E_k) and the rate of buoyancy or potential energy input (E_b). However, in industry under practical ladle refining conditions, gas flow rate is not appreciably high and thus one can neglect the contribution of kinetic energy (< 5%). So, the total energy input is practically equal to the rate of potential energy (E_b) input in the system [7]. Since $E \approx E_b$, it is expected that with increasing gas flow rate, more energy is imparted by the bubbles to the system. This leads to enhanced agitation and turbulence in the system, which in turn promotes mixing. Beyond a certain limit, increasing gas flow rate has almost no effect on the intensity of turbulence and the flow velocities do not change appreciably with gas flow rates Under such condition, mixing time is expected to change relatively weakly with the gas flow rates as shown in Figure 1.17[31]. Since potential energy input rate is directly proportional to the depth of liquid, consequently mixing time decreases with increasing liquid depth. However, a wider vessel is known to impair the rate of fluid mixing.
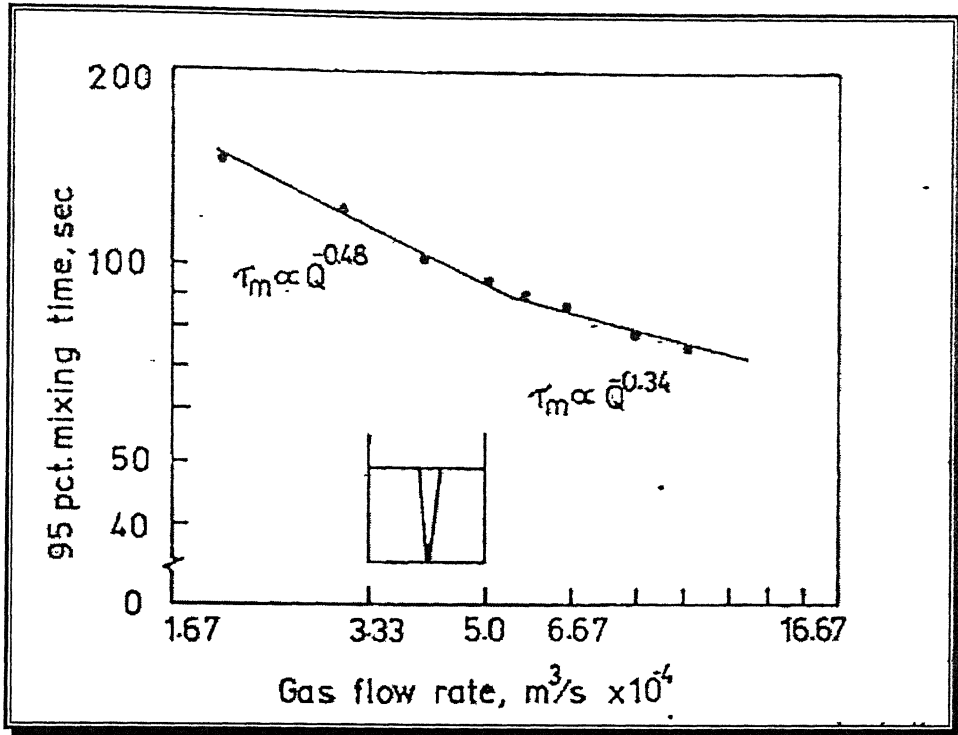
Figure 1.17: Experimentally measured mixing time in the water model ladle (L = 0.93m, R = 0.56m and β = 0.94) as a function of gas flow rates.

1.3 SCOPE OF THE PRESENT WORK

The injection of inert gases (N_2 and/or Argon) in ladles now-a-days becomes a common practice in steel making industry. Traditionally, the size of such processing ladles have only been moderate (often not exceeding 100 or 150 tonne) in which, argon is introduced through a single porous plug to stir the contents of the ladle. However, with increasing demand for refining of steel in large capacity ladles (up to about 500 tonnes), gas injection through a single porous plug is likely to be inadequate to ensure optimal stirring intensity in the bath. There is some practical limit on the gas flow rates that can be introduced through a single porous plug in ladle metallurgy steelmaking operation. As a consequence of such, inert gas stirring technology through twin plugs has been introduced and currently being increasing adopted by the industry for refining steel in relatively large

22

size ladles. The primary objective of this technique is to provide sufficient stirring thereby promoting the rates of various metallurgical processes without adversely affecting the general characteristics of the ladle refining operation (viz., minimal re-oxidation, negligible slag droplets entrainment/entrapment etc.). It is envisaged that in years to come, large size ladles will be necessitating dual plug bubbling in such systems for achieving superior product quality and better process economics [32].

Our main aim is to achieve the gentle but rapid mixing to promote metal/slag interaction, and to avoid explosive degassing effect under vacuum, splashing, spitting and entrapping non-metallic inclusion into bulk phase. To satisfy all the above conditions, dual plug bubbling is required. The literature review indicated that not much work on mixing in dual plug bubbling has been carried out. Indeed there are only two publications reported in the journal on this. These report contradicting findings, which are required to be resolved. Therefore the purpose of the present work is to carry out an extensive experimental investigation on ladle stirred with dual porous plugs.

1.4   LAYOUT OF THE THESIS

The main body of the thesis consists of five chapters. Chapter 1 presents a brief summery of the previous work done on mixing phenomena in cold models of industrial ladles. Chapter 2 presents the procedure of mixing time measurement and experimental results of mixing time as a function of gas flow rate, bath depth and vessel dimension in three different vessels. In Chapter 3, results in tabulated form are presented together with discussions. Chapter 4 summarizes the general conclusions derived from the present work and the thesis ends with the recommendation for future work in Chapter 5.

CHAPTER 2

EXPERIMENTAL WORK

2.1 INTRODUCTION

The intrinsic efficiencies of many chemical processing operations carried out in present day steelmaking ladles are intricately related to mixing phenomena [2, 33, 34, 35]. Mixing enhances chemical reactions as well as influences the extent of thermal, chemical and particle in-homogeneities of liquid steel within the ladles. To quantify mixing, mixing time has often been determined. The operating conditions prevalent in steel refining ladles are cumbersome. High temperatures, visual opacity of molten steel and massive size of industrial molten steel processing vessels pose difficulties for direct experimental observations. As it is impractical to carry out any elaborate studies in high temperature steel refining ladles, investigators for the last few decades were carrying out studies on many phenomenon such as fluid flow, mixing, mass transfer etc. laboratory scale models. Results were then scaled up for practical systems.

In this present study, mixing times in a twin plug stirred ladle was measured. Air/N_2 was injected through the bottom of three different cylindrical vessels filled with water using various combinations of nozzle(s) locations and gas flow rates. The present chapter describes the experimental measurements of mixing times under a wide variety of operating conditions.

2.2 THE FULL SCALE SYSTEM AND OPERATING CONDITIONS

The dimension of the full scale system together with the operating flow rates which was simulated in the laboratory is given in Table 2.1.

Table 2.1: Physical Dimensions of the Full Scale System.

Parameters of the Full Scale Ladle	
Vessel Capacity, tonne	150
Diameter at Base, m	3.65
Liquid Depth, m	3.04
Gas Injecting Device	Porous Plug
Number of Porous Plug	2
Dimensionless Porous Plug Location from the axis of the vessel	R/2 and R/3
Gas Flow Rate, m^3/s (Corrected to mean height and temperature of the liquid)	9.2×10^{-3} to 55.2×10^{-3}

With reference to the gas flow rate shown in Table 2.1 this was corrected with reference to operating temperature (1600°C) and mean hydrostatic pressure i.e. the hydrostatic pressure at mid bath depth.

2.3   SCALING DOWN AND THE THREE PHYSICAL MODELS

Three different Perspex tanks of cylindrical shape having different scale factors were fabricated respecting geometrical similarity with full scale system. The scale factors of three cylindrical vessels were 0.16, 0.13 and 0.08 with respect to the full scale 150 tonne ladle (Table 2.1). In each of these vessels, five nozzles were fitted at the bottom to facilitate gas injection. The nozzles were located at the centre, at (1/3) R, at - (1/3) R, at (1/2) R and at - (1/2) R locations. These allowed experiments to be carried out under various gas injection configurations. The physical dimensions of the three cylindrical shaped water model ladles are shown in Table 2.2.

Table 2.2: Physical Dimensions of Three Cylindrical Vessels.

Parameters	Vessel I (S.F. = 0.16)	Vessel II (S.F. = 0.13)	Vessel III (S.F. = 0.08)
Diameter, m	0.60	0.48	0.30
Depth, m	0.75	0.65	0.45
Nozzle Diameter, m	0.005	0.005	0.005
Plug Configurations at Diametrically Opposite Location	R/2, R/3, 0, -R/3 and -R/2	R/2, R/3, 0, -R/3 and -R/2	R/2, R/3, 0, -R/3 and -R/2
Total Gas Flow Rate, m^3/s	9.35×10^{-4} to 5.66×10^{-4}	0.55×10^{-4} to 3.37×10^{-4}	0.167×10^{-4} to 1.0×10^{-4}

S.F. = Scale Factor, defined by the ratio of the model diameter to the full scale diameter.

In addition to the three reduced scale cylindrical models, a tapered vessel was constructed with a scale factor of approximately 0.20 corresponding to the full scale ladle system of TATA steel respecting geometrical similarity. The model operating parameters deduced on the basis of Froude similarity criterion is shown in Table 2.3. There the full scale flow rates are first corrected to the mean height and operating temperature and subsequently translated into corresponding model flow rates using the scaling correlation $Q_{Model} = \lambda^{2.5} \times Q_{FS}$ [36]. All the gas flow rates in the reduced scale models are derived on the basis of the previously mentioned scaling equations, such that dynamic similarity between model and full scale systems are maintained.

Table 2.3: Physical Dimensions of the Tapered Vessel.

Parameters	Model (S.F. = 0.194)	Full Scale Ladle (TISCO)
Base Diameter, m	0.52	2.68
Top Diameter, m	0.58	2.99
Tapering Angle, degree	2.34	2.34
Liquid Depth, m	0.62	3.20
Dimension Porous Plug Location from the axis of the Vessel	0.58*	0.50
Range of Gas Flow Rates, m³/s (corrected to mean height and temperature of the liquid)	1.3×10^{-4} to 4.2×10^{-4}	8.05×10^{-3} to 25.14×10^{-3}

S.F. = Scale Factor, defined by the ratio of the model diameter to the full scale diameter.

* Marginally distorted.

2.4   EXPERIMENTAL SET UP FOR MIXING TIME MEASUREMENTS IN THE GAS STIRRED BATH

The schematic representation of laboratory scale experimental set up is shown in Figure 2.1. The experimental set up employed with three different cylindrical Perspex vessels having scale factor 0.16, 0.13 and 0.08 with respect to a full scale ladle of 150 tonne containing water at room temperature. In each of these vessels, nozzles were fitted at the bottom at various locations to facilitate gas injection into the water bath. The nozzles were located at the centre and at diametrically opposite positions at (1/3) R and (1/2) R respectively.

A tapered vessel with scale factor of approximately 0.20 of full scale ladle used in TISCO was also incorporated later. The nozzle locations were identified from the literature for optimal fluid flow and mixing conditions in the system [37]. All the vessels were kept inside a relatively bigger square crosses sectioned vessel. The space between the two tanks was filled with water to avoid optical distortions during the flow visualisation. The lower end of each vessel was sealed against the bottom of the square vessel by a neoprene gasket, applying pressure from the top to avoid any intermixing of water.

For the convenience of experimental study, all the three tanks together with two Rotameters and others were mounted in semi permanent steel super. In addition to this a lighting arrangement using 3X1000 W halogen bulbs contained in an air circulated aluminium box was fabricated on a rail immediately atop the super structure. The objective of this was to illuminate the central vertical plane of a vessel for direct visualization of flow in that plane.

Mixing times were measured in all the four vessels (three cylindrical vessels and one tapered vessel) as a function of liquid depth and gas flow rate using a EUTECH made CYBERSCAN 200 conductivity meter. Measurement of mixing times were carried out by

monitoring the changes in local concentration of a pulse tracer addition of approximately 3.5N KCl or 0.1N H_2SO_4. The tracer was added to the water bath at a point on the free surface in between the 'eyes' of the two surfacing plumes in case of dual plug configuration whereas in case of central plug axisymmetric bubbling it was added at the center of the 'eye' of the surfacing plume. The probe was located at a dimensionless position of 0.085 above the bottom wall and from the side wall of the ladle [38]. It is assumed that the tip of the probe was kept in the slowest mixing region so that measured 95% mixing times could be interpreted as bulk mixing times. The change in local ion concentration around the tip of the probe was measured through changes in the water's electrical conductivity and recorded via the conductivity meter coupled with a personal computer. The recording of the pulse tracer response was carried out until the concentration of the entire water bath was considered to have reached a homogeneous level. In the present study, the mixing time were estimated as the time required for the monitoring point concentration (or conductivity) to fall continuously within a $\pm$ 5% deviation band of the well mixed region. For each configuration four to five experiments were carried out and average mixing time was thereby determined. Variations between successive measurements and their associated average fall within 15% for Vessel I and Vessel II while for Vessel III it was around 30%. A typical tracer response curve is shown in Figure 2.2.

2.5   FLOW METERS AND THEIR CALIBRATION

Calibration of Rotameters (2.0 to 20.0 lits/min) has been done using a Wet-Test flow meter. The rotameter was calibrated against both air and N_2 shown in Figure 2.3(a) and Figure 2.3(b) respectively. The other rotameter ranging from 1.0 to 10.0 lits/min was standardized   against the calibrated rotameter by connecting the two in series.
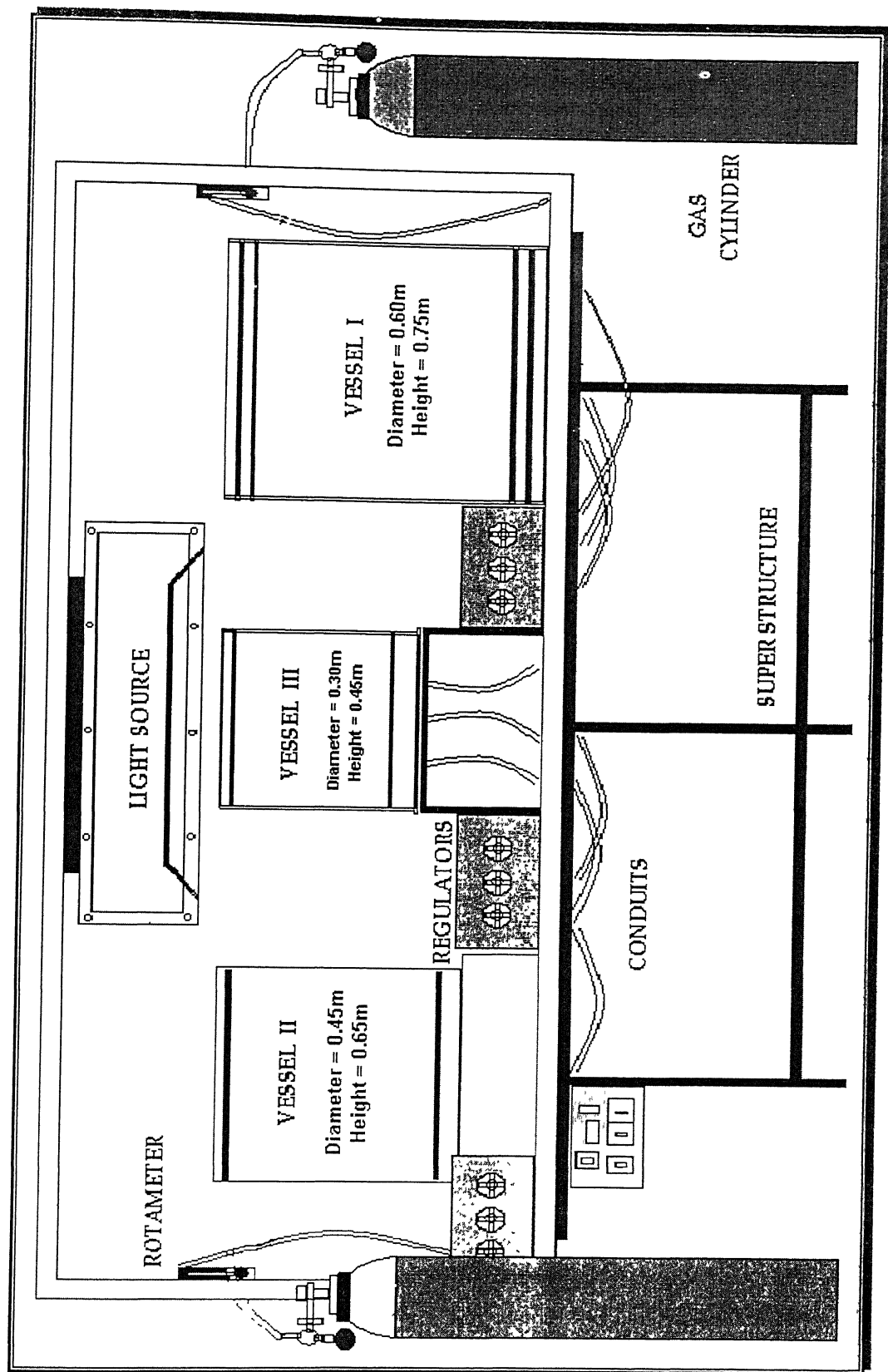
Figure 2.1: A schematic of laboratory scale experimental setup.
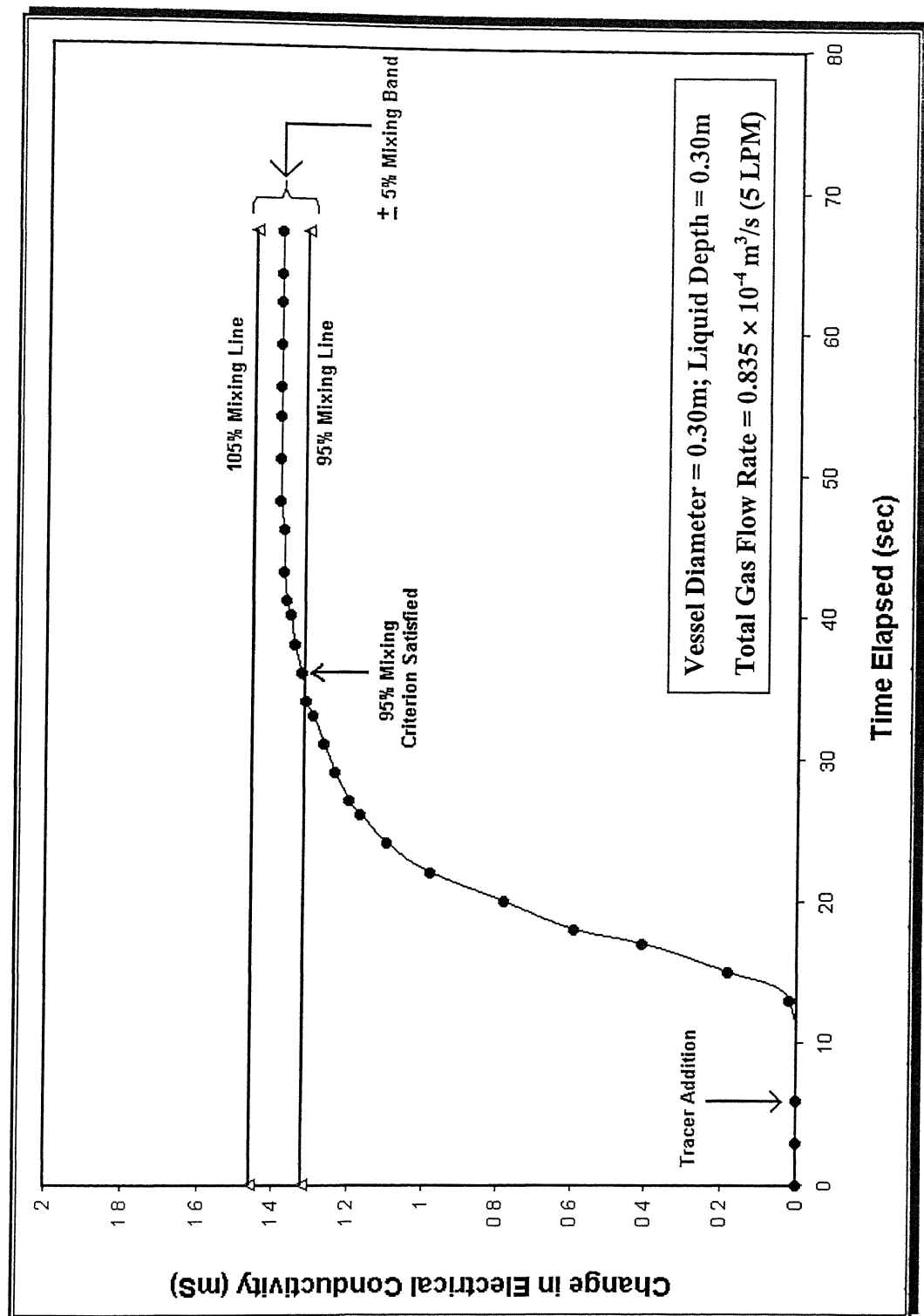
Figure 2.2: Experimentally measured variation of bath electrical conductivity at the monitoring point as a function of time.
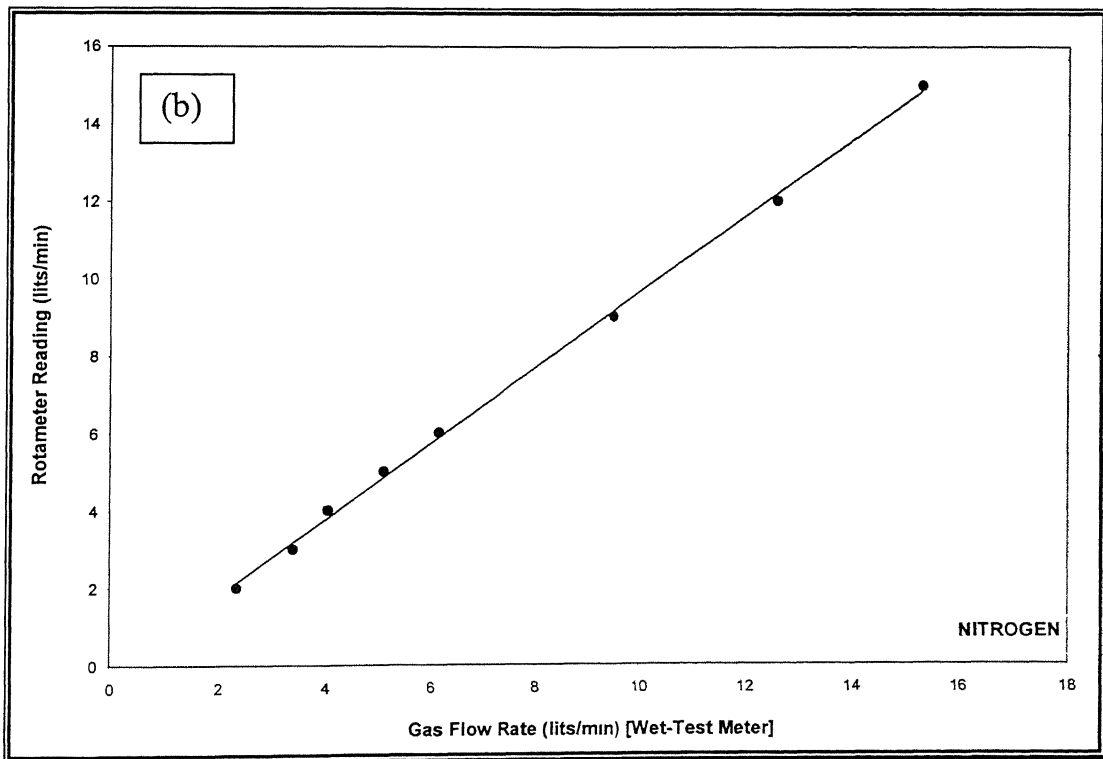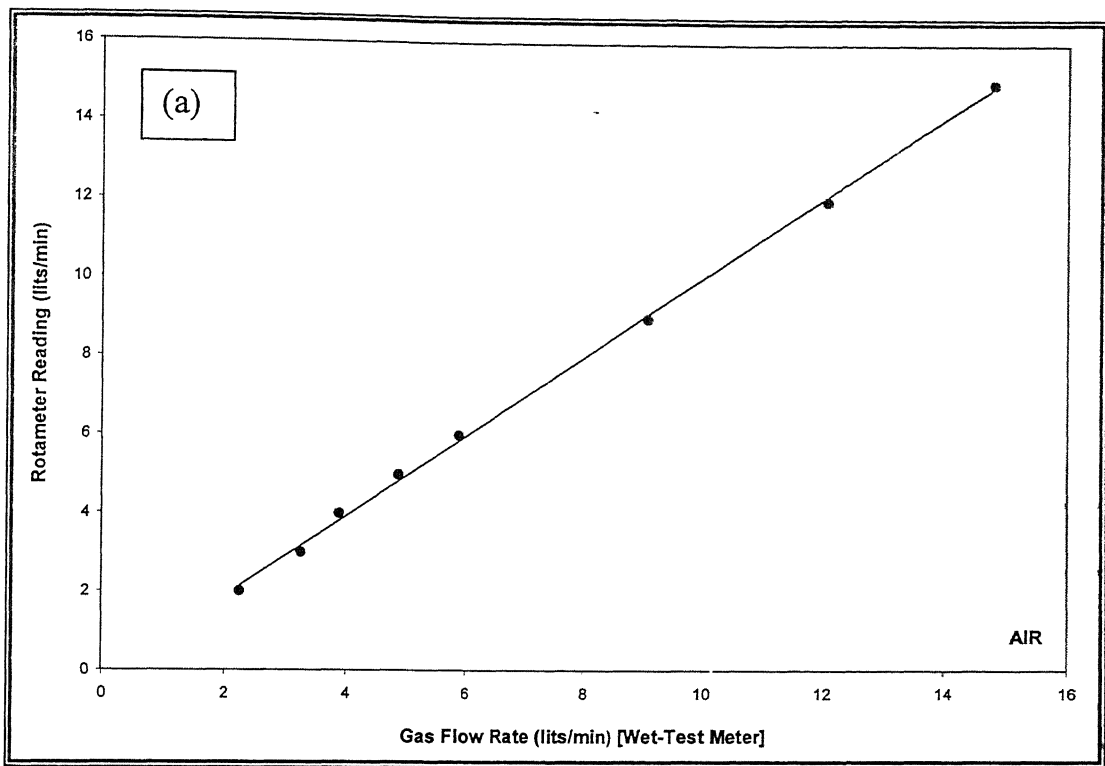
Figure 2.3: (a) Calibration curve in case of air.

(b) Calibration curve in case of nitrogen.

2.6 PROCEDURE FOR MIXING TIME MEASUREMENTS

Mixing times were measured in three different cylindrical vessels (I.D. = 0.60m, 0.48m and 0.30m) as well as in tapered vessel with bottom diameter 0.52m and tapering angle 2.34°, in which water bath was agitated by injecting air/N_2 through a pair of nozzles located at the bottom of the vessel. A few experiments were also carried out in Vessel I with axisymmetric plug location to assess the reliability of present measurements vis-à-vis a previously reported correlation of mixing time given in literature [33]. Two different nozzles configurations were investigated and these included, plugs located at diametrically opposite positions of (R/2) and (R/3) respectively. Before starting any measurements, air/N_2 was bubbled into the water bath at the specified flow rate for about 5 minutes to ensure the stability of the flow in the vessel as well as to homogenize the initial bath composition. Furthermore, the gas flow rates were so chosen to ensure gentle stirring condition as are encountered in actual ladle metallurgy steelmaking operations.
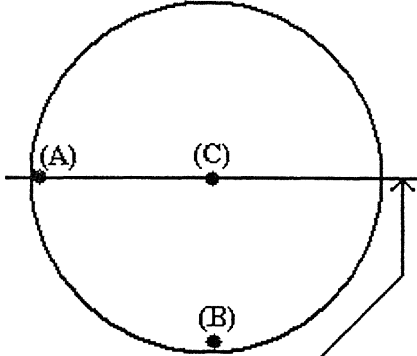
A conductivity probe supplied with digital conductivity meter was employed to record changes in the local ion concentration of pulse tracer (KCl or H_2SO_4) addition in the bath. The tracer was added at a point lying midway between the 'eyes' of surfacing plume [39]. The change in local ion concentration around the probe tip was measured through the changes in water's electrical conductivity and recorded manually via the digital conductivity meter as soon as change in electrical conductivity was shown on the monitor of the conductivity meter (typically every 2/3 seconds) and simultaneously stored in a computer using CyberComm Portable software. The recording of tracer response was carried out until the concentration was considered to have reached the homogeneously mixed value. On addition of tracer, considerable oscillations in the form of peaks and valleys were observed after plotting the recorded data's of change in electrical conductivity (mS) vs. time elapsed (s). These peaks and valleys result from the concentration fluctuations at the probe tip arising from inhomogeneities of the tracer concentration in the bath. In all experiments, the tip of the probe was kept at a location close to the bottom of the vessel and near the side wall and collinear with both the injection nozzles. The

measured time vs. conductivity data were analysed through MS-Excel® software for the estimation of mixing times as shown in Figure 2.2.

2.7 DETERMINATION OF PROBE LOCATION FOR REGISTERING BULK MIXING TIMES

The bulk mixing times (mixing times measured by immersing the probe in the slowest moving region) rather than local mixing times are a parameter of practical importance and there is no a-prior information on the region where mixing is slowest in the dual plug stirred system. Consequently, some experiments were carried out to determine the location of slowest mixing region in the dual plug stirred system such that the measured mixing time can be interpreted as the bulk mixing time. Mixing time measurements were carried out in Vessel I (D = 0.60m), keeping the probe at nine different locations for the flow rate of 2.83×10^{-4} m^3/s. Water was filled upto 0.60m of the vessel so as to keep the L/D ratio to 1. In Table 2.4 a summery of the experimental measurements is presented. It is clear from the table that mixing time is more rapid in regions close to the free surface whereas towards the base of the vessel mixing time is relatively sluggish. Furthermore, experimental results clearly indicate that registered mixing time is largest (and hence, measured mixing time is equivalent to bulk mixing time) provided the probe is located collinearly with the plugs near the vertical side of wall of about 0.025m from the vessel's bottom. In all the experiments, pulse tracer was added at a point lying midway between the 'eyes' of surfacing plume or in other words it was added through the bath free surface at a point immediately above the symmetry axis of the vessel. Consequently, for measured of mixing times reported in this thesis, tracer addition as well as the probe location was kept identical to those mentioned above.

Table 2.4: Mixing Times in Vessel I (D = 0.60m, L/D = 1.0 and Q = 2.83 × 10⁻⁴ m³/s)
for Various Locations of the Measuring Probe.

Probe Arrangement (Plan View)	Probe Height from the Bottom of the Vessel (m)	Probe Location	Average Mixing Times (s)
	0.025	A	30
		B	27
		C	23
	0.46	A	23
		B	22
		C	30
	0.53	A	19
		B	15
		C	20

Nozzles are located in this central vertical plane.

2.8 RELIABILITY OF EXPERIMENTAL MEASUREMENTS

Since the digital conductivity meter assembly was used to measure the mixing times in water model for the first time consequently, it is very important to assess the reliability of measurement technique. Thus it is necessary to compare the measured mixing times with similar measurements or correlation reported in the literature. To the end, 95% bulk mixing times were measured in Vessel I (D = 0.60m) as a function of gas flow rates and liquid depth for an axisymmetric gas injection configuration. Table 2.5 presents the experimental mixing time values for axisymmetric nozzle configuration in Vessel I (D = 0.60m).

Table 2.5: Mixing Time Values for Plug Located at the Centre of Vessel I (D = 0.60m)

L/D Ratio	Depth of Liquid (m)	Gas Flow Rate (lits/min)	Experimental Mixing Time (s)					Average Mixing Time (s)	Predicted Mixing Time (s)	Percentage Deviation*
			(i)	(ii)	(iii)	(iv)	(v)			
0.8	0.48	11.3	44.0	47.5	44.0	51.5	53.0	48.0	54.3	11.59
0.8	0.48	14.0	50.5	39.0	56.0	53.5	50.0	49.8	50.5	1.39
0.8	0.48	17.0	45.5	47.5	42.5	49.5	53.0	47.6	47.6	0
0.8	0.48	18.0	35.5	43.0	39.5	47.0	50.0	43.0	46.5	7.53
1.0	0.60	11.3	42.0	37.0	43.0	39.5	53.0	42.9	43.5	1.38
1 0	0.60	14.0	48.0	44.0	37.5	40.0	47.5	43.4	40.4	7.43
1.0	0.60	17.0	39.5	35.0	39.0	39.0	42.0	38.9	38.1	2.10
1.0	0.60	18.0	43.0	37.0	44.0	43.0	37.0	40.8	37.2	9.68
1.2	0.72	11.3	43.0	38.5	32.0	35.5	43.0	38.4	36.2	6.08
1.2	0.72	17.0	46.0	36.0	36.0	34.0	38.0	38.0	31.8	19.50

* Percentage Deviation $= \left| \dfrac{\tau_{mix,predicted} - \tau_{mix,measured}}{\tau_{mix,predicted}} \right| \times 100\%$

In Figure 2.4, a comparison of the average mixing times for various flow rates with derived mixing times from a well established correlation viz., $\tau_{mix, 95\%} = 25.4Q^{-0.33}L^{-1.0}R^{2.33}$ is shown. There, reasonable agreement between measurements and predictions evidently indicate the reliability of the model study program. It is instructive to note here that in order to have a comparison meaningful, tracer addition location as well as probe locations in these experiments were essentially kept similar to those, for which the macroscopic correlation was deduced.

2.9   REPRODUCIBILITY OF DATA

To check the reproducibility of the experimental measurements, these were repeated for four to five times under identical conditions of gas flow rate and L/D ratio. Figure 2.5 shows discrete experimental mixing time values as well as their average values for a set of four different experimental conditions in Vessel I. It is estimated from the above figure that the variation in mixing time, τ_{mix} between run to run was within $\pm$ 15% in all the cases.   Thus it can be concluded that fairly reproducible mixing time values were experimentally measured during the present investigation.

In Figure 2.6(a) and 2.6(b) the scatter in experimental measurements in Vessel II and Vessel III are shown respectively. The extent of data scatter ranged between 20 to 25% for the two vessels, which are somewhat higher than those shown for vessel I.
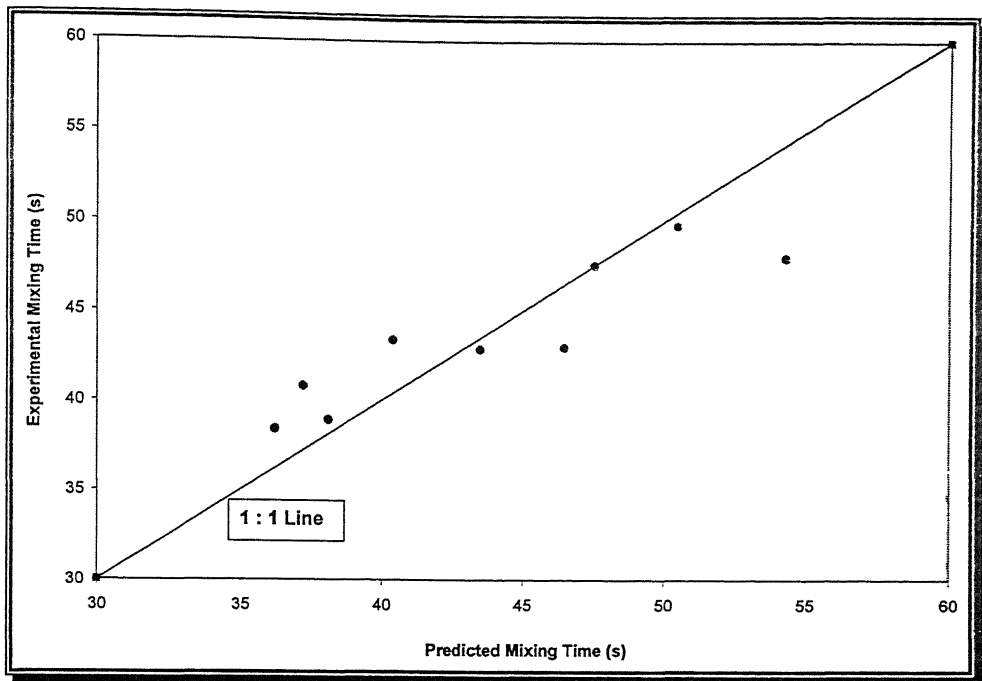
Figure 2.4: Experimentally measured mixing times in an axisymmetrical water model ladle (D=0.60m) for various operating conditions and their comparison with those deduced from an equivalent well known correlation.
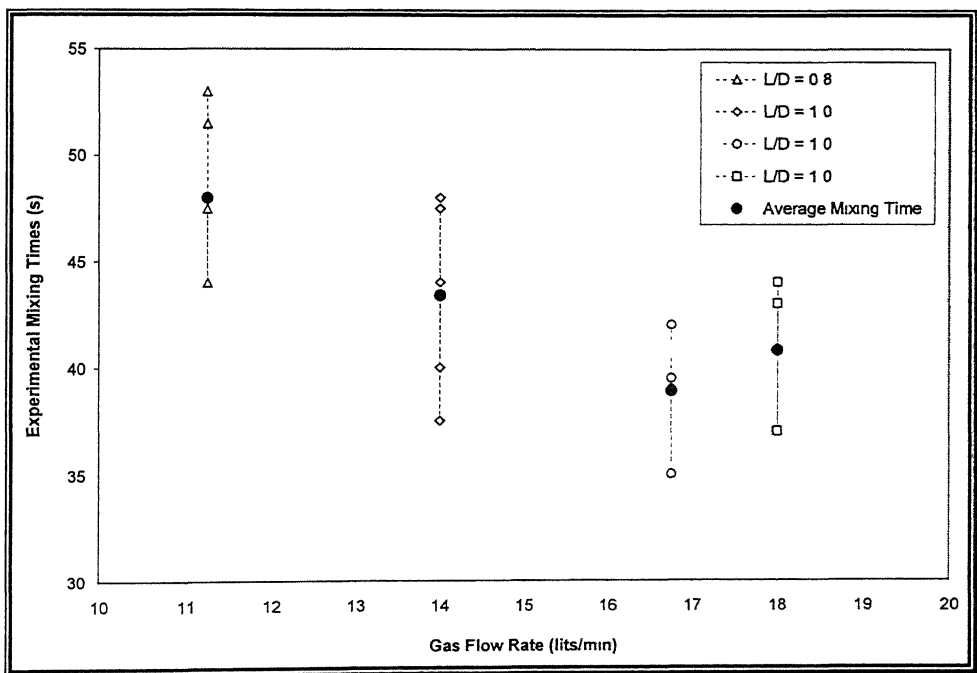
Figure 2.5: Experimentally measured mixing times in an axisymmetric water model ladle (D=0.60m) for various L/D ratios are plotted as a function of gas flow rates to check the deviation in measurement from one experiment to another. (For overlapping points only one is shown)

38
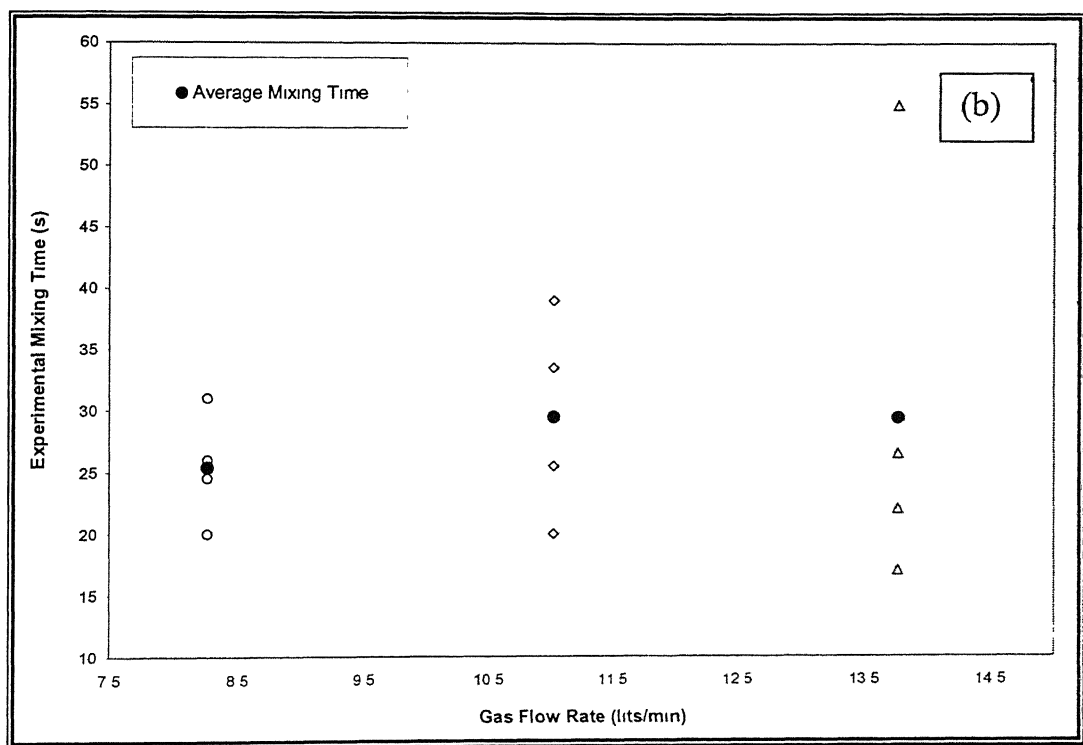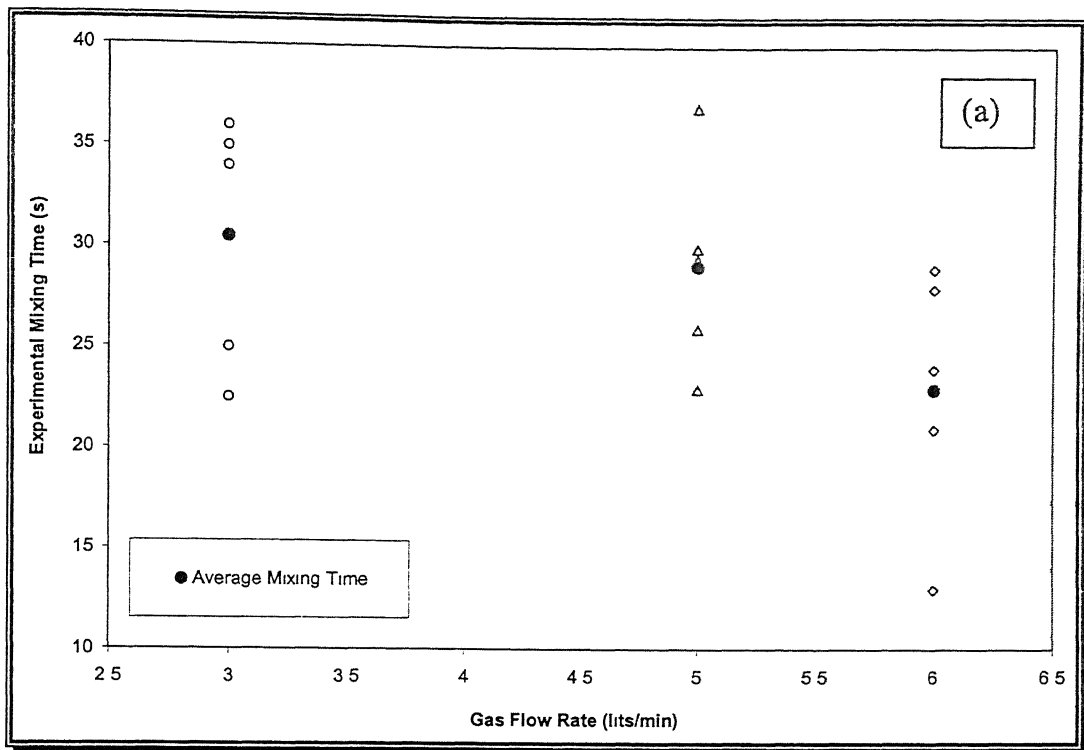
Figure 2.6: (a) Data Scatter in Vessel II (Diameter = 0.45m) for L/D = 1.0

(b) Data Scatter in Vessel III (Diameter = 0.30m) for L/D = 1.0

39

2.10 THE INFLUENCE OF DIFFERENT TYPES OF TRACER

Two types of tracer solution were used in the experimental work. Both the KCl and H_2SO_4 were extensively used for studying responses of pulse tracer in laboratory scale water model systems. The tracer was added in small amount at a point in the midway between the eyes of the surfacing plume. For the experimentally work approximately 3.5N KCl solution was used as a tracer at the beginning and later it was substituted with 0.1N dilute H_2SO_4 because of cost effectiveness (in the amount of tracer required was small). The measured mixing times values shows not much difference for the two types of tracer used. Table 2.6 presents influence of two types of tracer (KCl and H_2SO_4) on experimental mixing times for all the three vessels at a constant bath depth.

Table 2.6 : Influence of Tracer Types on Experimental Mixing Times for all the Three Vessels at a Fixed L/D Ratio of 1.0 and R/2 Nozzle Configuration.

	Total Gas Flow Rate (m^3/s)	Average Mixing Time (s)	
		KCl	H_2SO_4
Vessel I	0.50×10^{-4}	29.0	30.5
	0.84×10^{-4}	22.7	29.1
	1.00×10^{-4}	20.2	23.0
Vessel II	1.39×10^{-4}	34.3	25.4
	1.84×10^{-4}	32.1	29.5
	2.31×10^{-4}	30.4	29.4
Vessel III	1.89×10^{-4}	46.0	56.9
	2.84×10^{-4}	35.8	28.1
	3.34×10^{-4}	32.1	27.0

CHAPTER 3

RESULTS AND DISCUSSION

In this chapter experimental results of laboratory scale investigation and their discussion on various aspects are presented. Before taking any measurement on mixing times, Air/N$_2$ was blown into the water bath at the specific flow rates, scaled down from the industrial flow of a 150 tonne ladle, for 5 to 10 minutes to ensure the stability of flow in the vessel as well as to homogenize the initial bath composition. Also after each 15 to 20 experiments vessels were filled with new water substituting previous ionized water.

3.1 MIXING TIME FOR DIAMETRICALLY OPPOSITE R/3 PLUG POSITIONS AND DEVELOPMENT OF CORRELATION

In Table 3.1(a), Table 3.2(a) and Table 3.3(a) the experimental mixing times are presented for Vessel I (D = 0.60m), Vessel II (D = 0.48m) and Vessel III (D = 0.30m) respectively for various flow rates. Average mixing times for each configuration are calculated from a set of individual experimental mixing times. Assuming flow phenomena in typical gas stirred systems are dominated by the inertial and gravitational forces [33], a dimensional analysis has been carried out to establish a functional relationship between the key operating parameters namely, the gas flow rate, Q (in m^3/s), the liquid depth, L (in metre) and the mean radius of the vessel, R (in metre) along with gravitational acceleration, g (in m/s^2). The key operating parameters are related to mixing time according to.

$$\tau_{mix} = f(Q, L, R, g) \qquad (3.1)$$

Three different Π groups or dimensionless numbers are derived from Equation (3.1) according to Raleigh's method of indices. These are,

i) The dimensionless mixing time, $\left(\dfrac{\tau_{mix}^{2} g}{R} \right)$

ii) The geometrical aspect ratio, $\left(\dfrac{L}{R} \right)$

iii) The dimensionless gas flow rate, $\left(\dfrac{Q^{2}}{gR^{5}} \right)$

On the basis of the dimensionless numbers Equation (3.1) can be rewritten in the following non-dimensional form:

$$\frac{\tau_{mix}^{2} g}{R} = C_{0} \left(\frac{L}{R} \right)^{a} \left(\frac{Q^{2}}{gR^{5}} \right)^{b} \tag{3.2}$$

in which, C_{0}, a, b are dimensionless constants. The dimensionless pre-exponent C_{0} is a function of the mode of gas injection (symmetrical or asymmetrical), the degree of mixing, the location of tracer injection, the monitoring point, etc.

By carrying out multiple linear regression analysis of the experimental data (Table 3.1(b), Table 3.2(b) and Table 3.3(b)) using POLYMATH software, an explicit set of values for C_{0}, a and b in Equation (3.2) were deduced. In case of R/3 configuration of dual nozzles located diametrically opposite to each other, the correlation becomes:

$$\frac{\tau_{mix}^{2} g}{R} = 3008.8 \left(\frac{L}{R} \right)^{-0.94} \left(\frac{Q^{2}}{gR^{5}} \right)^{-0.27} \tag{3.3}$$

From this, 95% mixing time as an explicit function of the three key operating variables, viz. Q, L and R can be expressed as:

$$\tau_{mix, 95\%} = 23.9 \, Q^{-0.27} L^{-0.47} R^{1.65} \tag{3.4}$$

The value of multiple regression correlation coefficient [40] comes around 0.34 whereas root mean square deviation and variance (for definition see APPENDIX) shows

very small value of 0.029 and 0.034 respectively. For a reliable model variance and root mean square deviation should be as small as possible whereas the value of multiple regression correlation coefficient should approach to unity. The fitting of a model however should never simply be judged by the multiple regression correlation coefficient value above.

In Figure 3.1 maximum limit of certainty/uncertainty of the derived correlation in case of dual nozzles located at diametrically opposite position at R/3 is also shown. This indicates the extent of deviation of experimental data points to that of the predicted one range in between + 23.6% and − 43.2%. These values are comparable or even better than one proposed in the literature for axisymmetric gas stirred ladle system. Flow phenomena in gas stirred ladle systems are essentially transient in nature. The short term and long term wondering of bubbles release and escape of bubbles introduces unsteadiness in the system and therefore measure mixings are likely to vary from run to run. It is because of inherent fluctuation of the system, the data scatter is relatively pronounced in Figure 3.1. Such scatter, as one would note, are common for gas stirred systems as has been reported in the literature.
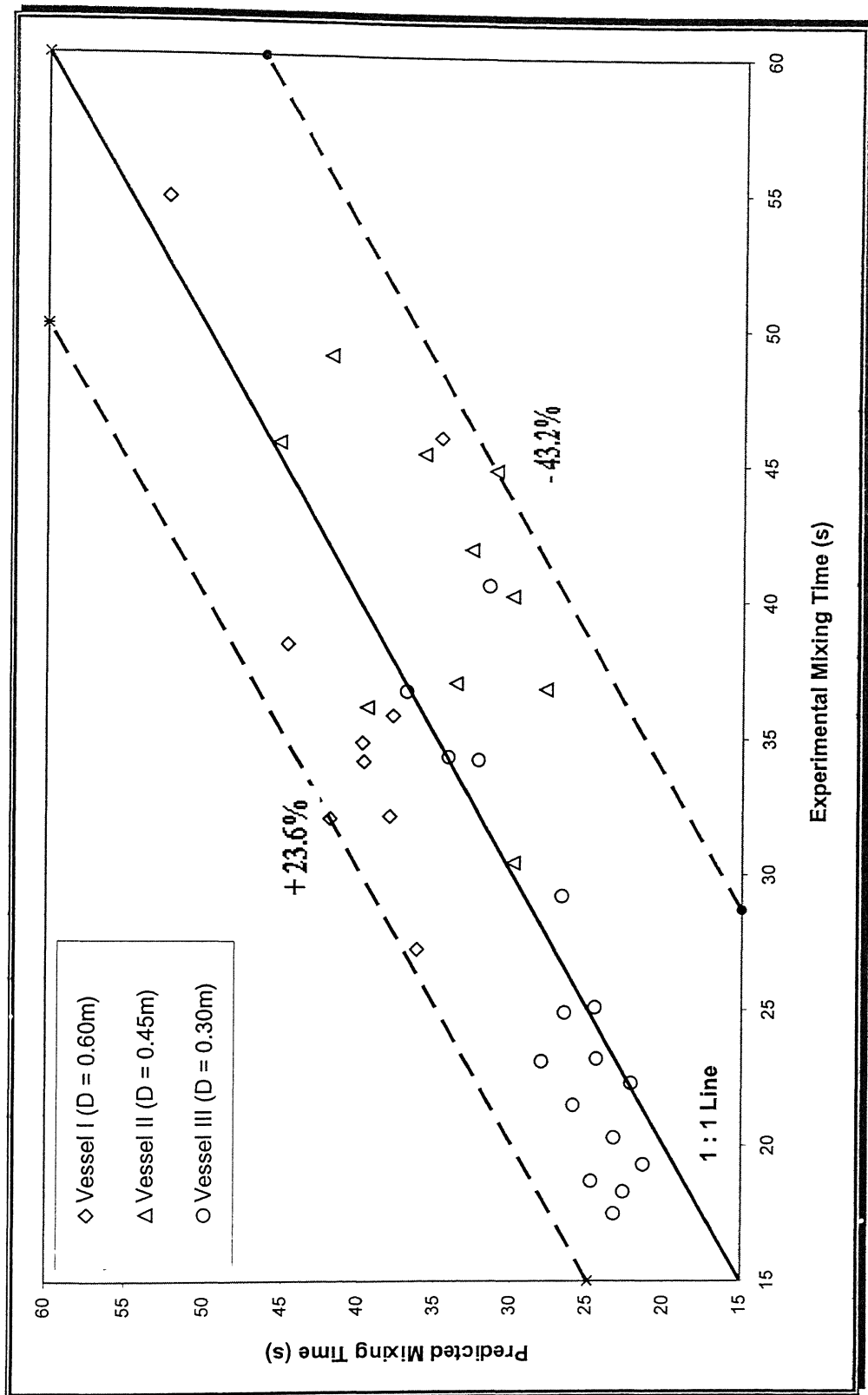
Figure 3.1: Maximum limit of certainty/uncertainty of the derived correlation in the case of dual nozzle configured at diametrically opposite R/3 positions.

44

Table 3.1(a): Experimentally Observed Mixing Time Values for Nozzles Located at Diametrically Opposite Position of R/3 in Vessel I (D = 0.60m).

L/D Ratio	Depth of Liquid (m)	Gas Flow Rate (lits/min)	Gas Flow Rate (m³/s)	Experimental Mixing Time (s)					Average Mixing Time (s)
				(i)	(ii)	(iii)	(iv)	(v)	
0.5	0.30	17.0	2.839×10^{-4}	38.5	63.0	57.5	60.0	55.0	54.8
0.7	0.42	17.0	2.839×10^{-4}	54.0	36.5	27.5	35.5	38.5	38.4
0.9	0.54	14.0	2.338×10^{-4}	36.0	36.0	25.5	39.0	23.5	32.0
0.9	0.54	17.0	2.839×10^{-4}	39.5	21.0	37.0	39.0	34.0	34.1
0.9	0.54	20.0	3.334×10^{-4}	33.0	35.0	20.5	31.0	41.0	32.1
1.0	0.60	14.0	2.338×10^{-4}	37.0	29.0	38.0	37.0	33.0	34.8
1 0	0.60	17.0	2.839×10^{-4}	33.5	40.5	28.5	36.0	40.5	35.8
1.0	0.60	20.0	0.835×10^{-4}	25.0	19.5	31.5	31.0	29.0	27.2
1.2	0.72	17.0	3.334×10^{-4}	49.5	46.5	49.0	38.0	47.0	46.0

Table 3.1(b): Predicted Mixing Times derived from a correlation in case of Vessel I (D = 0.60m) with Nozzles Located at Diametrically Opposite Position at R/3.

(L/D) Ratio	Total Gas Flow Rate, $Q \times 10^{-4}$ (m³/s)	Average Mixing Time, τ_{mix} (s)	$\left(\dfrac{\tau_{mix}^2 g}{R}\right)$	$\left(\dfrac{L}{R}\right)$	$\left(\dfrac{Q^2}{gR^5}\right)$	$\log\left(\dfrac{\tau_{mix}^2 g}{R}\right)$	$\log\left(\dfrac{L}{R}\right)$	$\log\left(\dfrac{Q^2}{gR^5}\right)$	Predicted Mixing Time (s)
0.5	2.839	54.8	98199.408	1.0	3.3811×10^{-06}	4.992108870	0	-5.470944496	52.4
0.7	2.839	38.4	48218.112	1.4	3.3811×10^{-06}	4.683210201	0.146128036	-5.470944496	44.7
0.9	2.338	32.0	33484.800	1.8	2.2931×10^{-06}	4.524847709	0.255272505	-5.639586267	41.9
0.9	2.839	34.1	38023.887	1.8	3.3811×10^{-06}	4.580056511	0.255272505	-5.470944496	39.7
0.9	3.334	32.1	33694.407	1.8	4.6797×10^{-06}	4.527557817	0.255272505	-5.329782347	38.0
1.0	2.338	34.8	39601.008	2.0	2.2931×10^{-06}	4.597706241	0.301029996	-5.639586267	39.8
1.0	2.839	35.8	41909.628	2.0	3.3811×10^{-06}	4.622313806	0.301029996	-5.470944496	37.8
1.0	0.835	27.2	24192.768	2.0	4.6797×10^{-06}	4.383685561	0.301029996	-5.329782347	36.2
1.2	3.334	46.0	69193.200	2.4	3.3811×10^{-06}	4.840063416	0.380211242	-5.470944496	34.7

46

Table 3.2(a): Experimentally Observed Mixing Time Values for Nozzles Located at Diametrically Opposite Position of R/3 in Vessel II (D = 0.45m).

L/D Ratio	Depth of Liquid (m)	Gas Flow Rate (lits/min)	Gas Flow Rate (m³/s)	Experimental Mixing Time (s)					Average Mixing Time (s)
				(i)	(ii)	(iii)	(iv)	(v)	
0.5	0.225	8.3	1.386×10^{-4}	40.5	47.0	45.0	50.5	46.0	45.8
0.5	0.225	11.0	1.837×10^{-4}	44.0	54.0	48.0	44.0	55.0	49.0
0.5	0.225	13.8	2.305×10^{-4}	48.0	36.0	29.0	31.5	36.0	36.1
0.7	0.315	11.0	1.837×10^{-4}	43.5	44.5	56.0	37.5	45.5	45.4
0.7	0.315	13.8	2.305×10^{-4}	42.0	32.0	42.0	25.0	44.0	37.0
0.9	0.405	10.0	1.667×10^{-4}	42.0	51.0	31.5	41.0	44.0	41.9
0.9	0.405	12.0	2.004×10^{-4}	48.0	46.0	49.0	33.0	48.0	44.8
0.9	0.405	13.8	2.305×10^{-4}	19.5	37.5	35.5	35.0	24.5	30.4
1.0	0.450	10.0	1.667×10^{-4}	36.0	62.5	49.0	41.0	48.5	47.4
1.0	0.450	12.0	2.004×10^{-4}	23.0	53.0	48.5	51.5	56.0	46.4
1.2	0.540	8.3	1.386×10^{-4}	26.0	66.0	32.0	37.0	40.0	40.2
1.2	0.540	11.0	1.837×10^{-4}	39.0	41.0	37.5	40.5	26.0	36.8

Table 3.2(b): Predicted Mixing Times derived from a correlation in case of Vessel II (D = 0.45m) with Nozzles Located at Diametrically Opposite Position at R/3.

(L/D) Ratio	Total Gas Flow Rate, $Q \times 10^{-4}$ (m³/s)	Average Mixing Time, τ_{mix} (s)	$\left(\dfrac{\tau_{mix}^2 g}{R}\right)$	$\left(\dfrac{L}{R}\right)$	$\left(\dfrac{Q^2}{gR^5}\right)$	$\log\left(\dfrac{\tau_{mix}^2 g}{R}\right)$	$\log\left(\dfrac{L}{R}\right)$	$\log\left(\dfrac{Q^2}{gR^5}\right)$	Predicted Mixing Time (s)
0.5	1.386	45.8	91457.104	1.0	3.3963×10^{-06}	4.961217445	0	-5.468992471	45.3
0.5	1.837	49.0	104683.600	1.0	5.9654×10^{-06}	5.019878649	0	-5.224363285	41.9
0.5	2.305	36.1	56819.956	1.0	9.3888×10^{-06}	4.754500893	0	-5.027390483	39.5
0.7	1.837	45.4	89866.576	1.4	5.9654×10^{-06}	4.953598195	0.146128036	-5.224363285	35.8
0.7	2.305	37.0	59688.400	1.4	9.3888×10^{-06}	4.775889937	0.146128036	-5.027390483	33.7
0.9	1.667	41.9	76544.596	1.8	4.9301×10^{-06}	4.883914535	0.255272505	-5.307148656	32.7
0.9	2.004	44.8	87506.944	1.8	7.0993×10^{-06}	4.942042517	0.255272505	-5.148786164	31.1
0.9	2.305	30.4	40293.376	1.8	9.3888×10^{-06}	4.605233656	0.255272505	-5.027390483	29.9
1.0	1.667	47.4	97958.736	2.0	4.9301×10^{-06}	4.991043173	0.301029996	-5.307148656	31.1
1.0	2.004	46.4	93869.056	2.0	7.0993×10^{-06}	4.972522450	0.301029996	-5.148786164	29.6
1.2	1.386	40.2	70459.344	2.4	3.3963×10^{-06}	4.847938595	0.380211242	-5.468992471	30.0
1.2	1.837	36.8	59044.864	2.4	5.9654×10^{-06}	4.771182127	0.380211242	-5.224363285	27.8

Table 3.3(a): Experimentally Observed Mixing Time Values for Nozzles Located at Diametrically Opposite Position of R/3 in Vessel III (D = 0.30m).

L/D Ratio	Depth of Liquid (m)	Gas Flow Rate (lits/min)	Gas Flow Rate (m³/s)	Experimental Mixing Time (s)					Average Mixing Time (s)
				(i)	(ii)	(iii)	(iv)	(v)	
0.5	0.15	3.0	0.501×10^{-4}	36.0	50.0	39.5	29.0	29.0	36.7
0.5	0.15	4.0	0.668×10^{-4}	23.0	42.5	24.0	40.5	41.5	34.3
0.5	0.15	5.0	0.835×10^{-4}	44.0	29.0	32.0	30.5	35.5	34.2
0.7	0.21	3.0	0.501×10^{-4}	38.0	36.0	47.0	34.0	48.0	40.6
0.7	0.21	5.0	0.835×10^{-4}	24.5	20.0	33.0	22.0	25.0	24.9
0.9	0.27	3.0	0.501×10^{-4}	15.5	33.0	26.0	14.0	27.0	23.1
0.9	0.27	4.0	0.668×10^{-4}	20.0	13.0	18.0	22.5	34.0	21.5
0.9	0.27	5.0	0.835×10^{-4}	17.0	22.0	25.5	25.5	26.0	23.2
0.9	0.27	6.0	1.002×10^{-4}	26.5	17.5	23.0	18.0	16.5	20.3
1.0	0.30	3.0	0.501×10^{-4}	40.0	13.0	40.0	19.5	33.5	29.2
1.0	0.30	4.0	0.668×10^{-4}	14.5	23.0	26.0	10.0	20.0	18.7
1.0	0.30	5.0	0.835×10^{-4}	29.0	19.5	10.0	19.0	10.0	17.5
1.0	0.30	6.0	1.002×10^{-4}	24.0	29.0	14.5	15.0	29.0	22.3
1.2	0.36	3.0	0.501×10^{-4}	23.0	24.0	18.5	35.0	25.0	25.1
1.2	0.36	4.0	0.668×10^{-4}	22.0	18.5	23.0	10.0	18.0	18.3
1.2	0.36	5.0	0.835×10^{-4}	8.5	24.5	22.5	23.0	18.0	19.3

Table 3.3(b): Predicted Mixing Times derived from a correlation in case of Vessel III (D = 0.30m) with Nozzles Located at Diametrically Opposite Position at R/3.

(L/D) Ratio	Total Gas Flow Rate, $Q \times 10^{-4}$ (m³/s)	Average Mixing Time, τ_{mix} (s)	$\dfrac{\tau_{mix}^2 g}{R}$	$\left(\dfrac{L}{R}\right)$	$\left(\dfrac{Q^2}{gR^5}\right)$	$\log\left(\dfrac{\tau_{mix}^2 g}{R}\right)$	$\log\left(\dfrac{L}{R}\right)$	$\log\left(\dfrac{Q^2}{gR^5}\right)$	Predicted Mixing Time (s)
0.5	0.501	36.7	88086.606	1.0	3.3694×10^{-06}	4.944909877	0	-5.472449851	36.9
0.5	0.668	34.3	76942.446	1.0	5.9900×10^{-06}	4.886165988	0	-5.222572378	34.2
0.5	0.835	34.2	76494.456	1.0	9.3594×10^{-06}	4.883629960	0	-5.028752352	32.2
0.7	0.501	40.6	107802.744	1.4	3.3694×10^{-06}	5.032629815	0.146128036	-5.472449851	31.5
0.7	0.835	24.9	40548.654	1.4	9.3594×10^{-06}	4.607976443	0.146128036	-5.028752352	26.5
0.9	0.501	23.1	34898.094	1.8	3.3694×10^{-06}	4.542801708	0.255272505	-5.472449851	28.0
0.9	0.668	21.5	30231.150	1.8	5.9900×10^{-06}	4.480454668	0.255272505	-5.222572378	25.9
0.9	0.835	23.2	35200.896	1.8	9.3594×10^{-06}	4.546553718	0.255272505	-5.028752352	24.4
0.9	1.002	20.3	26950.686	1.8	13.478×10^{-06}	4.430569824	0.255272505	-4.870389860	23.2
1.0	0.501	29.2	55762.656	2.0	3.3694×10^{-06}	4.746343451	0.301029996	-5.472449851	26.7
1.0	0.668	18.7	22869.726	2.0	5.9900×10^{-06}	4.359260961	0.301029996	-5.222572378	24.7
1.0	0.835	17.5	20028.750	2.0	9.3594×10^{-06}	4.301653846	0.301029996	-5.028752352	23.2
1.0	1.002	22.3	32522.766	2.0	13.478×10^{-06}	4.512187474	0.301029996	-4.870389860	22.1
1.2	0.501	25.1	41202.654	2.4	3.3694×10^{-06}	4.614925191	0.380211242	-5.472449851	24.5
1.2	0.668	18.3	21901.806	2.4	5.9900×10^{-06}	4.340479928	0.380211242	-5.222572378	22.6
1.2	0.835	19.3	24360.846	2.4	9.3594×10^{-06}	4.386692366	0.380211242	-5.028752352	21.3

3.2 MIXING TIME FOR DIAMETRICALLY OPPOSITE R/2 PLUG POSITIONS AND DEVELOPMENT OF CORRELATION

The same procedure as described above, in Section 3.1 is adopted for derivation of an appropriate correlation of mixing time in case of dual nozzles located at R/2 positions located diametrically opposite to each other. In this case the correlation generated has the form:

$$\frac{\tau_{mix}^{2} g}{R} = 2842.2 \left(\frac{L}{R}\right)^{-1.04} \left(\frac{Q^2}{gR^5}\right)^{-0.28} \tag{3.5}$$

From this, 95% mixing time as an explicit function of the three key operating variables, viz. Q, L and R can be expressed as:

$$\tau_{mix,\,95\%} = 23.4\,Q^{-0.28}\,L^{-0.52}\,R^{1.72} \tag{3.6}$$

The value of multiple regression correlation coefficient here in this case comes around 0.44 as compared to 0.34 in the case of R/3 dual nozzle configuration which indicates better fit of the correlation derived for R/2 dual nozzle configuration over the correlation derived for R/3 nozzle configuration. The root mean square deviation and variance [40] shows very small value of 0.027 and 0.033 respectively.

Table 3.4(a), Table 3.5(a) and Table 3.6(a) show the experimental mixing times for Vessel I (D = 0.60m), Vessel II (D = 0.48m) and Vessel III (D = 0.30m) respectively for various flow rates. Average mixing times for each configuration are calculated from a set of experimental mixing times. Table 3.4(b), Table 3.5(b) and Table 3.6(b) summerises the estimated dimensionless groups for various operating condition.

In Figure 3.2 maximum limit of certainty/uncertainty of the derived correlation in case of dual nozzles located at diametrically opposite position at R/2 has been shown. The deviation of experimental mixing times to predicted mixing times are ranges in between

51

+25.9% and − 33.9%. In comparison with R/3, R/2 nozzle configurations generates less deviations, in other words we can conclude that for R/2 dual nozzle configuration the fitted correlation describes experimental observations relatively more closely.

On the basis of Figure 3.1 and Figure 3.2, it can be seen that the extent of data scatter with respect to the 1:1 fitted straight line is more pronounced for R/3 dual nozzle configuration. Generally, the extent of data scatter is related to the following [39],

i)   Bigger L/D ratio, as the bubble plume wandering increases with increase in liquid depth

ii)   Greater specific gas flows, as any increase in gas flows for a given mass of Liquid increases free surface disturbances and thus, tend to impart more unsteadiness to the system

iii)   Closer proximity of the two nozzles at the base of the vessels, since plume-plume interactions becomes more pronounced with closer plugs, leading to enhanced flow fluctuations.
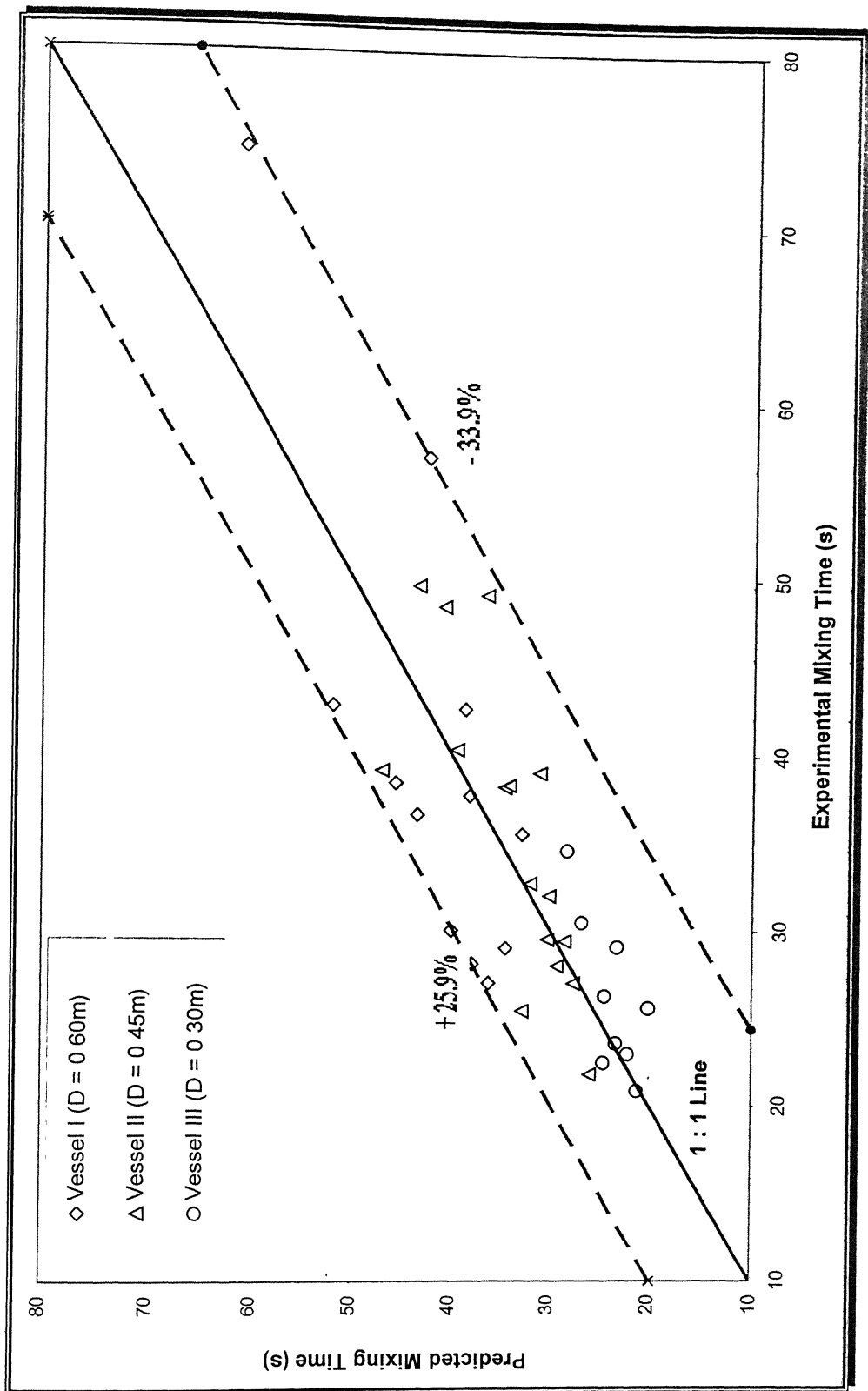
Figure 3.2: Maximum limit of certainty/uncertainty of the derived correlation in the case of dual nozzle configured at diametrically opposite R/2 positions.

Table 3.4(a): Experimentally Observed Mixing Time Values for Nozzles Located at Diametrically Opposite Position of R/2 in Vessel I (D = 0.60m).

L/D Ratio	Depth of Liquid (m)	Gas Flow Rate (lits/min)	Gas Flow Rate (m³/s)	Experimental Mixing Time (s)					Average Mixing Time (s)
				(i)	(ii)	(iii)	(iv)	(v)	
0.5	0.30	11.3	1.887×10^{-4}	29.5	63.0	76.0	87.5	116.5	74.5
0.5	0.30	17.0	2.839×10^{-4}	44.5	36.5	19.5	61.0	27.0	37.7
0.5	0.30	20.0	3.334×10^{-4}	85.0	28.5	24.0	31.0	45.5	42.8
0.7	0.42	11.3	1.887×10^{-4}	45.0	72.0	86.5	96.0	50.0	69.9
0.7	0.42	17.0	2.839×10^{-4}	54.5	40.0	23.5	39.5	34.5	38.4
0.7	0.42	20.0	3.334×10^{-4}	25.0	38.5	36.0	29.5	54.0	36.6
0.9	0.54	11.3	1.887×10^{-4}	93.5	86.0	27.0	71.5	44.0	64.4
0.9	0.54	17.0	2.839×10^{-4}	42.5	30.0	23.5	26.0	28.0	30.0
0.9	0.54	20.0	3.334×10^{-4}	24.0	31.0	39.0	45.0	49.5	37.7
1.0	0.60	11.3	1.887×10^{-4}	72.5	66.5	53.5	44.5	47.5	56.9
1.0	0.60	14.0	2.338×10^{-4}	25.0	23.0	26.5	25.5	20.0	24.0
1.0	0.60	17.0	2.839×10^{-4}	34.0	37.0	22.5	20.0	27.0	28.1
1.0	0.60	20.0	3.334×10^{-4}	22.5	35.0	31.0	22.0	24.5	27.0
1.2	0.72	11.3	1.887×10^{-4}	41.5	28.0	43.0	56.5	44.0	42.6
1.2	0.72	17.0	2.839×10^{-4}	22.0	27.5	32.5	31.0	32.0	29.0
1.2	0.72	20.0	3.334×10^{-4}	26.0	31.0	37.0	42.0	41.5	35.5

Table 3.4(b): Predicted Mixing Times derived from a correlation in case of Vessel I (D = 0.60m) with Nozzles Located at Diametrically Opposite Position at R/2.

(L/D) Ratio	Total Gas Flow Rate, $Q \times 10^{-4}$ (m³/s)	Average Mixing Time, τ_{mix} (s)	$\left(\dfrac{\tau_{mix}^2 g}{R}\right)$	$\left(\dfrac{L}{R}\right)$	$\left(\dfrac{Q^2}{gR^5}\right)$	$\log\left(\dfrac{\tau_{mix}^2 g}{R}\right)$	$\log\left(\dfrac{L}{R}\right)$	$\log\left(\dfrac{Q^2}{gR^5}\right)$	Predicted Mixing Time (s)
0.5	1.887	74.5	181493.175	1.0	1.494×10^{-6}	5.258860298	0	-5.825685452	61.0
0.5	2.839	37.7	46476.183	1.0	3.361×10^{-6}	4.667230453	0	-5.473502934	54.4
0.5	3.334	42.8	59901.168	1.0	4.680×10^{-6}	4.777435291	0	-5.329782347	51.9
0.7	1.887	69.9	159772.527	1.4	1.494×10^{-6}	5.203502104	0.146128036	-5.825685452	51.2
0.7	2.839	38.4	48218.112	1.4	3.361×10^{-6}	4.683210201	0.146128036	-5.473502934	45.6
0.7	3.334	36.6	43803.612	1.4	4.680×10^{-6}	4.641509923	0.146128036	-5.329782347	43.5
0.9	1.887	64.4	135618.672	1.8	1.494×10^{-6}	5.132319487	0.255272505	-5.825685452	44.9
0.9	2.839	30.0	29430.000	1.8	3.361×10^{-6}	4.468790262	0.255272505	-5.473502934	40.0
0.9	3.334	37.7	46476.183	1.8	4.680×10^{-6}	4.667230453	0.255272505	-5.329782347	38.2
1.0	1.887	56.9	105869.847	2.0	1.494×10^{-6}	5.024772285	0.301029996	-5.825685452	42.5
1.0	2.338	24.0	18835.200	2.0	2.293×10^{-6}	4.274970236	0.301029996	-5.639586267	40.0
1.0	2.839	28.1	25820.247	2.0	3.361×10^{-6}	4.411960392	0.301029996	-5.473502934	37.9
1.0	3.334	27.0	23838.300	2.0	4.680×10^{-6}	4.377275281	0.301029996	-5.329782347	36.2
1.2	1.887	42.6	59342.652	2.4	1.494×10^{-6}	4.773366951	0.380211242	-5.825685452	38.7
1.2	2.839	29.0	27500.700	2.4	3.361×10^{-6}	4.439343748	0.380211242	-5.473502934	34.5
1.2	3.334	35.5	41210.175	2.4	4.680×10^{-6}	4.615004459	0.380211242	-5.329782347	32.9

Table 3.5(a): Experimentally Observed Mixing Time Values for Nozzles Located at Diametrically Opposite Position of R/2 in Vessel II (D = 0.45m).

L/D Ratio	Depth of Liquid (m)	Gas Flow Rate (lits/min)	Gas Flow Rate (m³/s)	Experimental Mixing Time (s)					Average Mixing Time (s)
				(i)	(ii)	(iii)	(iv)	(v)	
0.5	0.225	8.3	$1.386 \times 10\text{-}4$	68.0	42.0	24.0	23.5	38.0	39.1
0.5	0.225	11.0	$1.837 \times 10\text{-}4$	60.5	69.5	35.0	55.0	28.0	49.6
0.5	0.225	13.8	$2.305 \times 10\text{-}4$	45.5	48.0	48.5	54.0	46.0	48.4
0.7	0.315	8.3	$1.386 \times 10\text{-}4$	47.5	33.5	45.0	28.5	47.0	40.3
0.7	0.315	11.0	$1.837 \times 10\text{-}4$	67.0	69.0	38.5	30.0	41.0	49.1
0.7	0.315	13.8	$2.305 \times 10\text{-}4$	40.5	41.0	23.0	40.0	47.0	38.3
0.9	0.405	8.3	$1.386 \times 10\text{-}4$	26.5	52.0	42.0	47.5	23.0	38.2
0.9	0.405	11.0	$1.837 \times 10\text{-}4$	21.0	35.5	30.0	29.0	48.0	32.7
0.9	0.405	13.8	$2.305 \times 10\text{-}4$	47.5	22.0	24.0	45.5	21.0	32.0
1.0	0.450	8.3	$1.386 \times 10\text{-}4$	25.5	20.0	26.0	31.0	24.5	25.4
1.0	0.450	10.0	$1.667 \times 10\text{-}4$	37.0	43.0	32.5	39.5	43.0	39.0
1.0	0.450	11.0	$1.837 \times 10\text{-}4$	33.5	39.0	20.0	25.5	29.5	29.5
1.0	0.450	13.8	$2.305 \times 10\text{-}4$	26.5	17.0	22.0	26.5	55.0	29.4
1.2	0.540	8.3	$1.386 \times 10\text{-}4$	21.0	21.0	23.5	35.0	39.5	28.0
1.2	0.540	11.0	$1.837 \times 10\text{-}4$	34.5	17.0	18.0	32.5	33.0	27.0
1.2	0.540	13.8	$2.305 \times 10\text{-}4$	24.5	17.5	28.0	18.0	21.0	21.8

Table 3.5(b): Predicted Mixing Times derived from a correlation in case of Vessel II (D = 0.45m) with Nozzles Located at Diametrically Opposite Position at R/2.

(L/D) Ratio	Total Gas Flow Rate, $Q \times 10^{-4}$ (m³/s)	Average Mixing Time, τ_{mix} (s)	$\left(\dfrac{\tau_{mix}^2 g}{R}\right)$	$\left(\dfrac{L}{R}\right)$	$\left(\dfrac{Q^2}{gR^5}\right)$	$\log\left(\dfrac{\tau_{mix}^2 g}{R}\right)$	$\log\left(\dfrac{L}{R}\right)$	$\log\left(\dfrac{Q^2}{gR^5}\right)$	Predicted Mixing Time (s)
0.5	1.386	39.1	66656.116	1.0	3.368×10^{-06}	4.823840004	0	-5.47266294	47.0
0.5	1.837	49.6	107262.976	1.0	5.993×10^{-06}	5.030449842	0	-5.222391459	43.4
0.5	2.305	48.4	102135.616	1.0	9.355×10^{-06}	5.009177213	0	-5.028965441	40.8
0.7	1.386	40.3	70810.324	1.4	3.368×10^{-06}	4.850096582	0.146128036	-5.47266294	39.5
0.7	1.837	49.1	105111.316	1.4	5.993×10^{-06}	5.021649474	0.146128036	-5.222391459	36.5
0.7	2.305	38.3	63956.404	1.4	9.355×10^{-06}	4.805884037	0.146128036	-5.028965441	34.2
0.9	1.386	38.2	63622.864	1.8	3.368×10^{-06}	4.803613215	0.255272505	-5.47266294	34.6
0.9	1.837	32.7	46621.044	1.8	5.993×10^{-06}	4.668581995	0.255272505	-5.222391459	32.0
0.9	2.305	32.0	44646.400	1.8	9.355×10^{-06}	4.649786446	0.255272505	-5.028965441	30.1
1.0	1.386	25.4	28128.976	2.0	3.368×10^{-06}	4.449153923	0.301029996	-5.47266294	32.8
1.0	1.667	39.0	66315.600	2.0	4.93×10^{-06}	4.821615703	0.301029996	-5.307148656	31.1
1.0	1.837	29.5	37942.900	2.0	5.993×10^{-06}	4.579130521	0.301029996	-5.222391459	30.3
1.0	2.305	29.4	37686.096	2.0	9.355×10^{-06}	4.576181150	0.301029996	-5.028965441	28.5
1.2	1.386	28.0	34182.400	2.4	3.368×10^{-06}	4.533802552	0.380211242	-5.47266294	29.3
1.2	1.837	27.0	31784.400	2.4	5.993×10^{-06}	4.502214018	0.380211242	-5.222391459	27.6
1.2	2.305	21.8	20720.464	2.4	9.355×10^{-06}	4.316399476	0.380211242	-5.028965441	25.9

Table 3.6(a): Experimentally Observed Mixing Time Values for Nozzles Located at Diametrically Opposite Position of R/2 in Vessel III (D = 0.30m).

L/D Ratio	Depth of Liquid (m)	Gas Flow Rate (lits/min)	Gas Flow Rate (m³/s)	Experimental Mixing Time (s)					Average Mixing Time (s)
				(i)	(ii)	(iii)	(iv)	(v)	
0.9	0.27	3.0	0.501×10^{-4}	37.0	38.0	40.5	35.0	22.5	34.6
0.9	0.27	5.0	0.835×10^{-4}	35.5	24.5	14.5	22.5	15.5	22.5
0.9	0.27	6.0	1.002×10^{-4}	26.5	25.5	11.0	30.0	25.0	23.6
1.0	0.30	3.0	0.501×10^{-4}	35.0	34.0	36.0	25.0	22.5	30.5
1.0	0.30	5.0	0.835×10^{-4}	26.0	29.5	37.0	30.0	23.0	29.1
1.0	0.30	6.0	1.002×10^{-4}	28.0	21.0	29.0	24.0	13.0	23.0
1.2	0.36	3.0	0.501×10^{-4}	23.0	18.0	37.5	22.0	31.0	26.3
1.2	0.36	5.0	0.835×10^{-4}	39.0	14.5	10.0	18.0	23.0	20.9
1.2	0.36	6.0	1.002×10^{-4}	24.0	29.5	29.5	24.0	21.0	25.6

58

Table 3.6(b): Predicted Mixing Times derived from a correlation in case of Vessel III (D = 0.30m) with Nozzles Located at Diametrically Opposite Position at R/2.

(L/D) Ratio	Total Gas Flow Rate, $Q \times 10^{-4}$ (m³/s)	Average Mixing Time, τ_{mix} (s)	$\left(\dfrac{\tau_{mix}^2 g}{R}\right)$	$\left(\dfrac{L}{R}\right)$	$\left(\dfrac{Q^2}{gR^5}\right)$	$\log\left(\dfrac{\tau_{mix}^2 g}{R}\right)$	$\log\left(\dfrac{L}{R}\right)$	$\log\left(\dfrac{Q^2}{gR^5}\right)$	Predicted Mixing Time (s)
0.9	0.501	34.6	78294.264	1.8	3.369×10^{-6}	4.893729946	0.255272505	-5.472449851	28.3
0.9	0.835	22.5	33108.750	1.8	9.359×10^{-6}	4.519942785	0.255272505	-5.028752352	24.5
0.9	1.002	23.6	36425.184	1.8	13.480×10^{-6}	4.561401754	0.255272505	-4.870389860	23.3
1.0	0.501	30.5	60838.350	2.0	3.369×10^{-6}	4.784177427	0.301029996	-5.472449851	26.8
1.0	0.835	29.1	55381.374	2.0	9.359×10^{-6}	4.743363726	0.301029996	-5.028752352	23.2
1.0	1.002	23.0	34596.600	2.0	13.480×10^{-6}	4.539033420	0.301029996	-4.870389860	22.1
1.2	0.501	26.3	45236.526	2.4	3.369×10^{-6}	4.655489245	0.380211242	-5.472449851	24.4
1.2	0.835	20.9	28567.374	2.4	9.359×10^{-6}	4.455870321	0.380211242	-5.028752352	21.2
1.2	1.002	25.6	42860.544	2.4	13.480×10^{-6}	4.632057679	0.380211242	-4.870389860	20.1

3.3 ADEQUACY OF THE CORRELATIONS WITH RESPECT TO THE PREVIOUSLY REPORTED EXPERIMENTAL WORK

To assess the derived correlations described above in Section 3.1 and Section 3.2 and their adequacy, the experimentally measured mixing times reported by Joo and Guthrie [28] were examined. In Table 3.7, a comparison between measured and predicted mixing times are shown for two different nozzle locations, namely R/2 and R/3 at diametrically opposite positions for various gas flow rates. Joo and Guthrie did their experiments to measure the mixing times keeping the monitoring point of the conductivity probe immersed at a position immediately above the bottom of their vessel along the line of symmetry. But in our experiments the probe location was completely different at a dimensionless position of 0.085 above the bottom wall and from the vessel side wall. As the measured mixing times are sensitive to probe location (Table 2.4) the predicted mixing times based on the original correlation derived in Section 3.1 and Section 3.2 gives somewhat longer mixing time than the measured one [28]. Results presented in Table 2.4 indicate that the measured mixing times for probe location at "A" (applied in present work) are somewhat longer (by a factor of 1.3 (= 30/23)) than the probe location at "C" (applied by Joo and Guthrie). To validate the above correlations for probe location used by Joo and Guthrie, one should accordingly reduce the pre–exponents in Equation (3.4) and (3.6) by a factor of 1.3. The predicted mixing times thus obtained are shown in Table 3.7 together with experimental measurements. There as seen, agreement between measurements and prediction appear reasonable (well within the limit of uncertainty of the correlations).

Table 3.7: Predicted Mixing Times for Two Different Nozzle Locations for Various Gas Flow Rates and their Comparison with those Measured Experimentally by Joo and Guthrie [28].

Nozzle Locations (Dual Nozzle at Diametrically Opposite Position)	Gas Flow Rate (lits/min)	Gas Flow Rate (m^3/s)	Experimental Mixing Times (s)	Predicted Mixing Times (s)		Percentage Deviation* (Reported)
				Based on Original Value of the Pre-exponent	Based on Modified Value of the Pre-exponent	
R/2 Position	10	1.67×10^{-4}	73	81.4	62.6	16.6
	20	3.34×10^{-4}	49	67.1	51.6	5.0
	30	5.01×10^{-4}	35	59.9	46.1	24.1
	40	6.68×10^{-4}	29	55.2	42.5	31.8
R/3 Position	10	1.67×10^{-4}	80	79.4	61.1	30.9
	20	3.34×10^{-4}	56	65.8	50.6	10.7
	30	5.01×10^{-4}	45	59.0	45.4	0.9
	40	6.68×10^{-4}	36	54.6	42.0	14.3

*$\textbf{Percentage Deviation} = \dfrac{\left| \tau_{mix,predicted} - \tau_{mix,measured} \right|}{\tau_{mix,predicted}} \times 100\%$

3.4   THE ROLE OF TAPERING OF VESSEL ON MIXING

Industrial ladles are not purely cylindrical in shape but slightly tapered. The tapering angle mostly ranges within 5°. As shown already that taper causes a secondary recirculation motion in the bottom outside corner of a typical ladle [5] which influences mixing to some extent.
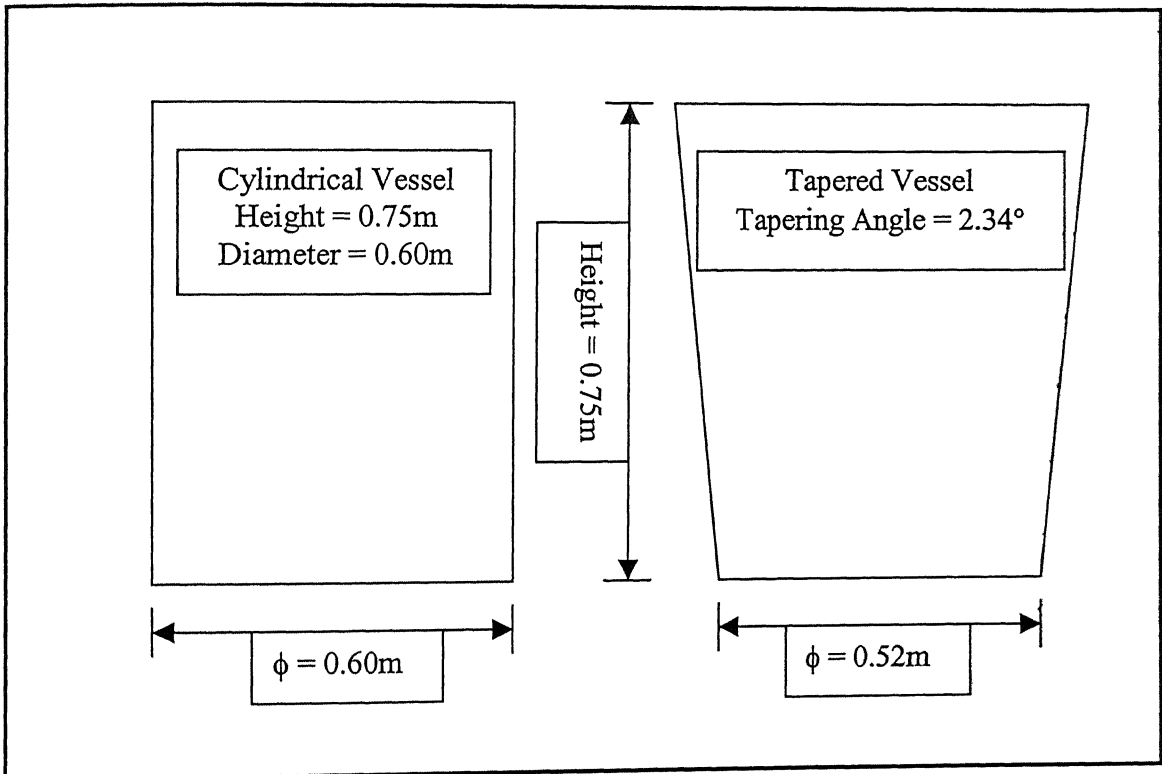
In case of cylindrical vessel the L/D ratio is defined simply by the ratio of liquid depth to the vessel diameter. For cylindrical vessel the diameter is always constant where as for the tapered vessel the effective diameter keeps on changing through out the vessel depth. The L/D ratio for the tapered vessel is defined as the ratio of liquid depth to the effective diameter. The effective diameter is a function of bath depth can be calculated in the following way:

Effective Diameter = 2 × Effective Radius (3.7)

Effective Radius = [(Base Radius + Radius at the corresponding Liquid Depth) / 2] (3.8)

Radius at the corresponding liquid depth can be calculated using the formula given below [41]:

Volume of liquid = [Π × H (R_0^2 + R_0 × R_B + R_B^2)] / 3 (3.9)

where R_0 is the radius of the vessel corresponding to liquid depth, in metre

R_B is the bottom radius of the vessel (= 0.26m),

and H is the bath depth, in metre.

3.4.1 Case I : L/D Ratio Same as that of the Cylindrical Vessel

In Table 3.8(a), the mixing times at various gas flow rates are shown in case of a tapered vessel (Bottom Diameter = 0.52m, Top Diameter = 0.58m and Tapered Angle = 2.34°) with L/D_{eff} ratios 0.7 and 1.0. The bath depth, L becomes 0.38m and 0.56m whereas the effective diameter, D_{eff} i.e., the diameter at the liquid surface becomes 0.55m and 0.56m for L/D_{eff} ratio of 0.7 and 1.0 respectively. The L/D ratios are calculated on the basis of effective diameter of the vessel. As the volume of the liquid in case of a tapered vessel is always less than that in cylindrical vessel with same L/D ratio, the stirring energy per unit mass in tapered vessel will be comparatively more. Therefore, the mixing time in case of tapered vessel becomes comparatively less, provided that the flow rate is maintained same. This is depicted in Figure 3.3 which shows that almost all the mixing time values are somewhat smaller than what should be the value of corresponding mixing time in case of cylindrical vessel. Also it is seen from Figure 3.3 that the values of experimental mixing times are lower than the deviation band shown in Figure 3.2. Furthermore, when the ladle is tapered the nozzles become located at 0.6R instead of 0.5. This may cause some uncertainty in extrapolating the correlation to tapered vessel. Table 3.8(b) shows calculated mixing time on the basis of R_{eff} for same L/D ratio as that of the cylindrical vessel.

3.4.2 Case II : Same Volume of Liquid as the Cylindrical Vessel

In Table 3.9(a), the mixing times at various gas flow rates are shown in case of tapered vessel (Bottom Diameter = 0.52m) with same volume of Liquid as the cylindrical vessel (D = 0.60m) corresponding to 0.7 and 1.0 L/D ratio. Vessel I (D = 0.60m) contains 0.12 m^3 and 0.17 m^3 of water for the L/D ratios of 0.7 and 1.0 respectively. The corresponding L/D ratios in case of tapered vessel become 0.93 and 1.24 respectively. As the volume of liquid is kept constant in both the cylindrical and the tapered vessel, the height of the liquid bath would be more in case of later one. The value of effective radius would not be change much with respect to bath depth because of very small tapered angle (2.34°). From the correlation for mixing time for the case of diametrically opposite R/2 nozzle locations, one can say that mixing time will be reduced with increasing bath depth. Now as the bath depth is more in case of tapered vessel for the same volume of Liquid the mixing time in case of tapered one would be less than that in case of cylindrical vessel. Figure 3.4 conveys the same message. Table 3.9(b) shows calculated mixing time on the basis of R_{eff} for constant volume of liquid as that in cylindrical vessel. Reasonable estimation between measurement and prediction is evident.
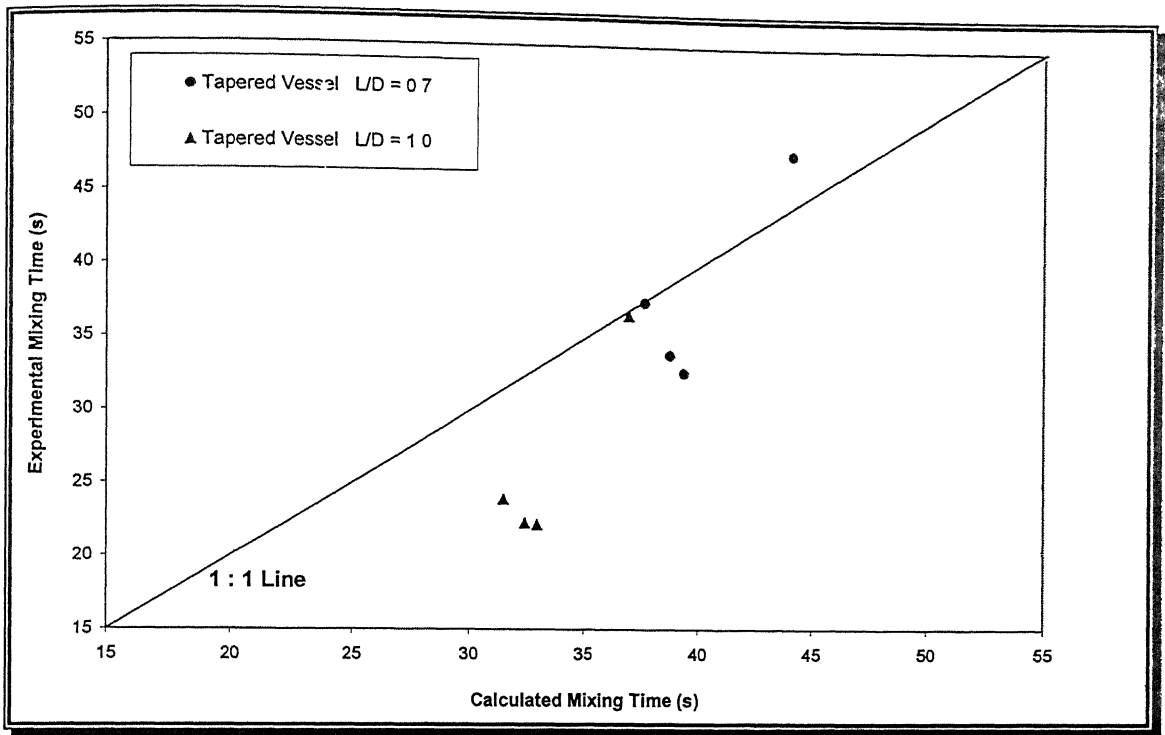
Figure 3.3: Experimental mixing time in case of tapered vessel with diametrically opposite dual nozzle configuration at a position of R/2 is plotted as a function of calculated mixing time $(23.4Q^{-0.28}L^{-0.52}R_{eff}^{1.72})$ for same L/D_{eff} ratio as that of the cylindrical vessel.
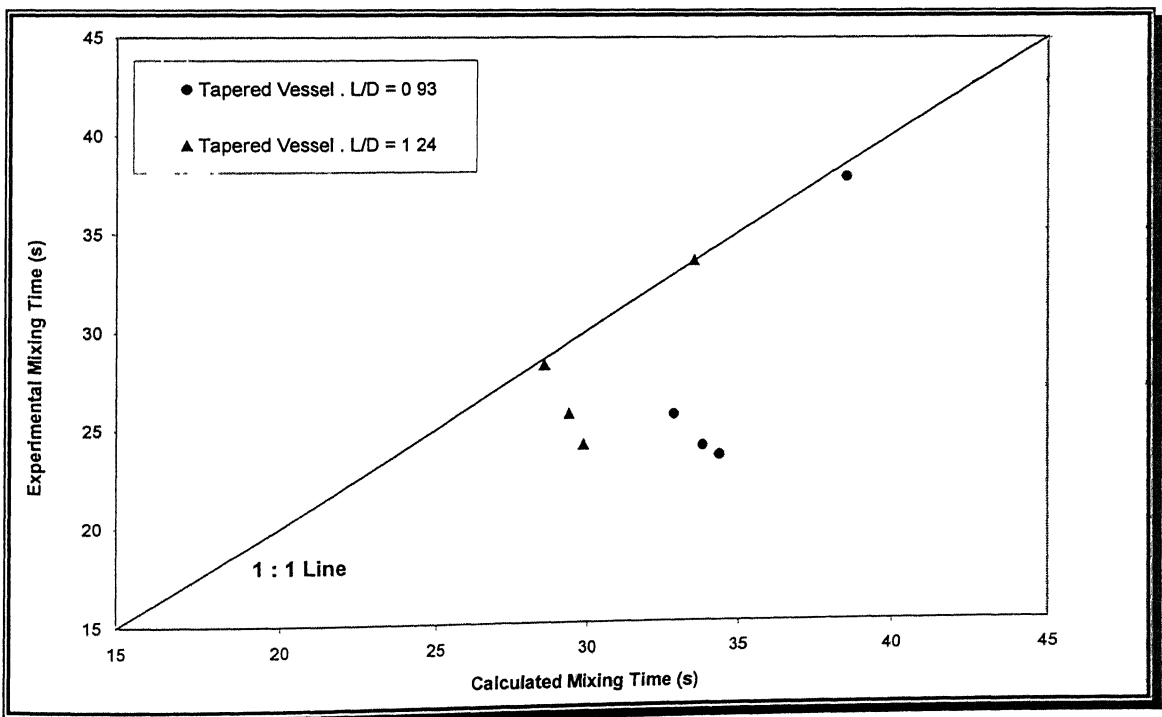
Figure 3.4: Experimental mixing time in case of tapered vessel with diametrically opposite dual nozzle configuration at a position of R/2 is plotted as a function of calculated mixing time $(23.4\ Q^{-0.28}L^{-0.52}R_{eff}^{1.72})$ for same volume of liquid as that in cylindrical vessel.

Table 3.8(a): Experimentally Observed Mixing Time Values for Nozzles Located at Position of R/2 Diametrically Opposite to Each Other in the Tapered Vessel (Base Diameter = 0.52m and Top Diameter = 0.58m) with Same L/D Ratio as that of Vessel I (D = 0.6m)

L/D Ratio	Liquid Depth (m)	Effective Diameter (m)	Total Gas Flow Rate (lits/min)	Total Gas Flow Rate, $Q \times 10^{-4}$ (m^3/s)	Experimental Mixing Time (s)					Average Mixing Time (s)	Mixing Time in Cylindrical Vessel (s)
					(i)	(ii)	(iii)	(iv)	(v)		
0.7	0.383	0.536	11.3	1.887	42.0	47.5	51.0	45.0	53.0	47.7	69.9
0.7	0.383	0.536	17.0	2.839	31.5	37.0	32.0	36.5	26.5	32.7	38.4
0.7	0.383	0.536	18.0	3.006	28.5	45.5	28.5	38.0	29.0	33.9	-
07	0.383	0.536	20.0	3.334	36.5	37.0	40.0	39.5	34.5	37.5	36.6
1.0	0.565	0.543	11.3	1.887	40.5	37.0	31.5	37.5	36.5	36.6	56.9
1.0	0.565	0.543	17.0	2.839	25.0	22.5	20.0	21.0	22.5	22.2	28.1
1.0	0.565	0.543	18.0	3.006	17.0	15.0	29.0	27.5	23.0	22.3	-
1.0	0.565	0.543	20.0	3.334	24.5	21.5	28.0	21.5	24.0	23.9	27.0

Table 3.8(b): Experimental mixing Times for Tapered Vessel Corresponding to Calculated Mixing Time $(23.4Q^{-0.28}L^{-0.52}R_{eff}^{1.72})$ Considering Same L/D Ratio as that of the Cylindrical Vessel.

Total Gas Flow Rate (m³/s) Q	Liquid Depth (m) L	Effective Radius (m) R_{eff}	Average Mixing Time (s) τ_{mix}	Calculated Mixing Time (s) $[23.4Q^{-0.28}L^{-0.52}R_{eff}^{1.72}]$
1.887×10^{-4}	0.383	0.26785	47.7	44.2
2.839×10^{-4}	0.383	0.26785	32.7	39.3
3.006×10^{-4}	0.383	0.26785	33.9	38.8
3.334×10^{-4}	0.383	0.26785	37.5	37.7
1.887×10^{-4}	0.565	0.27158	36.6	25.0
2.839×10^{-4}	0.565	0.27158	22.2	33.0
3.006×10^{-4}	0.565	0.27158	22.3	32.3
3.334×10^{-4}	0.565	0.27158	23.9	31.6

Table 3.9(a): Experimentally Observed Mixing Time Values for Nozzles Located at Position of R/2 Diametrically Opposite to Each Other in the Tapered Vessel (Base Diameter = 0.52m and Top Diameter = 0.58m) with Same Volume of Liquid as in Vessel I (D = 0.60m).

L/D$_{eff}$ Ratio	Depth of Liquid (m)	Effective Diameter (m)	Total Gas Flow Rate (lits/min)	Total Gas Flow Rate (m³/s)	Experimental Mixing Time (s)					Average Mixing Time (s)
					(i)	(ii)	(iii)	(iv)	(v)	
0.93	0.516	0.541	11.3	1.887×10^{-4}	41.0	38.0	43.0	33.0	34.0	37.8
0.93	0.516	0.541	17.0	2.839×10^{-4}	25.0	20.0	22.5	28.0	22.0	23.5
0.93	0.516	0.541	18.0	3.006×10^{-4}	24.0	22.0	26.5	25.0	22.5	24.0
0.93	0.516	0.541	20.0	3.334×10^{-4}	22.5	23.0	34.0	24.0	24.5	25.6
1.24	0.707	0.549	11.3	1.887×10^{-4}	28.0	36.0	39.0	31.0	33.5	33.5
1.24	0.707	0.549	17.0	2.839×10^{-4}	23.5	31.0	21.5	25.0	19.5	24.1
1.24	0.707	0.549	18.0	3.006×10^{-4}	19.5	28.0	22.5	29.0	29.5	25.7
1.24	0.707	0.549	20.0	3.334×10^{-4}	30.5	25.0	33.5	31.0	21.0	28.2

Table 3.9(b): Experimental mixing Times for Tapered Vessel Corresponding to Calculated Mixing Time $(23.4Q^{-0.28}L^{-0.52}R_{eff}^{1.72})$ Considering Same Volume of Liquid as in the Cylindrical Vessel.

Total Gas Flow Rate (m³/s) Q	Liquid Depth (m) L	Effective Radius (m) R_{eff}	Average Mixing Time (s) τ_{mix}	Calculated Mixing Time (s) $[23.4Q^{-0.28}L^{-0.52}R_{eff}^{1.72}]$
1.887×10^{-4}	0.516	0.27078	37.8	38.6
2.839×10^{-4}	0.516	0.27078	23.5	34.4
3.006×10^{-4}	0.516	0.27078	24.0	33.7
3.334×10^{-4}	0.516	0.27078	25.6	32.8
1.887×10^{-4}	0.707	0.27449	33.5	33.5
2.839×10^{-4}	0.707	0.27449	24.1	30.0
3.006×10^{-4}	0.707	0.27449	25.7	29.5
3.334×10^{-4}	0.707	0.27449	28.2	28.6

3.5 PERFORMANCE COMPARISON : DUAL VS. SINGLE PLUG

In Table 3.10 and Table 3.11 show the experimental mixing times for various gas flow rates in case of Vessel I (D = 0.60m) with nozzle(s) configuration at the line of symmetry and at R/2 position diametrically opposite to each other respectively. A plot of experimental mixing times against gas flow rates for both single and dual nozzle configuration is shown in Figure 3.5 and Figure 3.6. The mixing time for various operating conditions like the gas flow rate, Q, the liquid depth, L and the radius of the vessel, R in case of the dual nozzle configuration is less than that in case of the single axisymmetric nozzle configuration only above a critical flow rate as shown in Figure 3.5. However, below the critical flow rate axisymmetric nozzle configuration is more advantageous than dual nozzle configuration located at diametrically opposite R/2 positions. This is because of low stirring energy per unit mass of liquid. As the flow rates are low the stirring energy i.e. the specific energy input rate would be correspondingly low and in such a condition there exist a large slowly moving secondary vortex adjacent to the bottom and side wall of the ladle. This secondary vortex results in reduction of mixing time. Beyond the critical flow rate, the flow pattern essentially shifts to that of single recirculating vortex driven by the rising plume [31].

The log-log plot in Figure 3.6 shows the dependence of mixing time on gas flow rates for dual nozzle configuration. It can be said from Figure 3.6 that dependence of mixing time on gas flow rates for the case of dual nozzles is practically same (approximately 1/3 power) as that of axisymmetric nozzle beyond the critical flow rate, reported in literature [31].

Table 3.10: Mixing Times Values for Single Nozzle Located at the Line of Symmetry i.e., Axisymmetric Position for Constant Bath Depth in case of Cylindrical Vessel I (D = 0.60m).

L/D Ratio	Liquid Depth (m)	Gas Flow Rate (lits/min)	Gas Flow Rate (m³/s) $Q \times 10^{-4}$	Experimental Mixing Time (s)					Average Mixing Time (s)
				(i)	(ii)	(iii)	(iv)	(v)	
1.0	0.60	4.0	0.668	61.0	51.0	55.5	60.5	57.0	57.0
		6.0	1.002	53.0	64.5	54.0	40.0	53.5	53.0
		8.0	1.336	38.0	45.0	44.0	48.0	49.0	44.8
		10.0	1.667	42.0	42.0	45.0	39.5	42.0	42.1
		12.0	2.004	40.5	38.5	37.0	44.0	40.0	40.0
		16.0	2.672	42.0	26.0	34.0	53.0	38.0	38.6
		17.0	2.839	39.5	35.0	39.0	39.0	42.0	38.9
		20.0	3.334	34.5	35.0	45.0	35.0	37.5	37.4

Table 3.11: Mixing Times Values for Dual Nozzles Located at Diametrically Opposite R/2 Positions with Constant Bath Depth in case of Cylindrical Vessel I (D= 0.60m).

L/D Ratio	Liquid Depth (m)	Gas Flow Rate (lits/min)	Gas Flow Rate (m³/s) $Q \times 10^{-4}$	Experimental Mixing Time (s)					Average Mixing Time (s)
				(i)	(ii)	(iii)	(iv)	(v)	
1.0	0.60	4.0	0.668	59.0	58.5	53.0	58.5	68.0	59.4
		6.0	1.002	65.0	59.0	51.0	50.0	50.0	55.0
		8.0	1.336	50.0	60.0	48.5	46.0	47.0	50.3
		10.0	1.667	44.5	33.0	47.5	44.5	39.0	41.7
		12.0	2.004	38.5	35.5	38.0	28.0	41.5	36.3
		16.0	2.672	32.0	21.5	21.5	33.5	38.5	29.4
		17.0	2.839	34.0	37.0	22.5	20.0	27.0	28.1
		20.0	3.334	22.5	35.0	31.0	22.0	24.5	27.0

Figure 3.5: Experimentally measured mixing times in a 0.16 scale cylindrical water model ladle of 150 tonne full scale ladle (Diameter = 0.60m) as a function of gas flow rate.
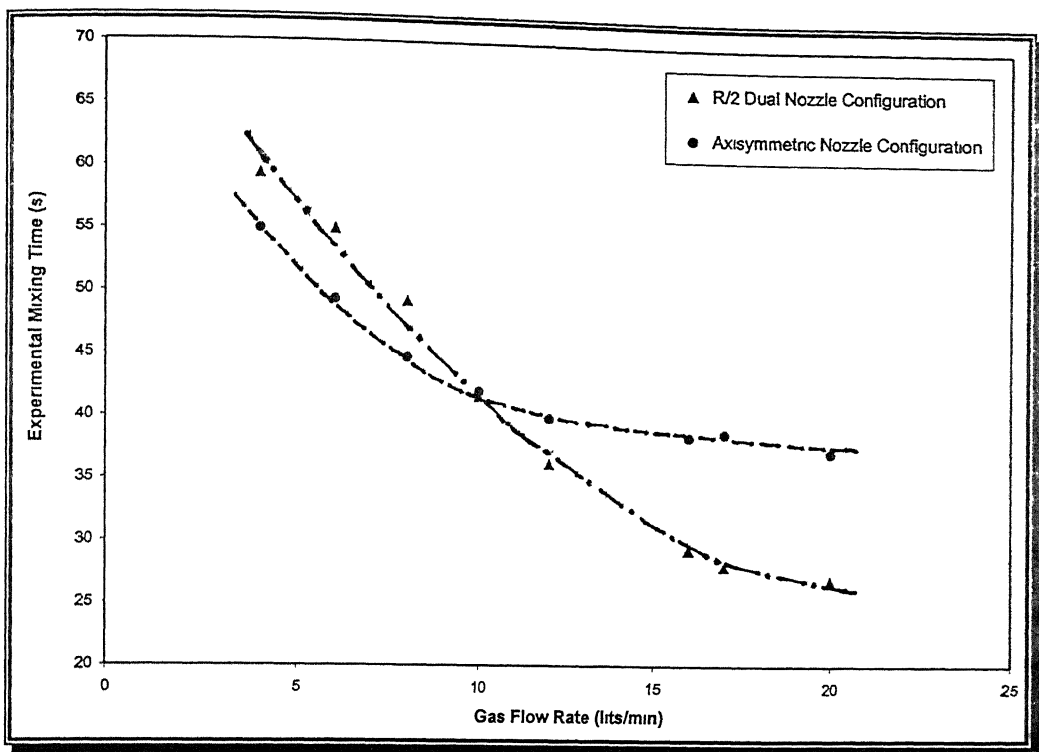

Figure 3.6: Experimentally measured mixing times in a 0.16 scale cylindrical water model ladle of 150 tonne full scale ladle (Diameter = 0.60m) as a function of gas flow rate. [log-log Scale]
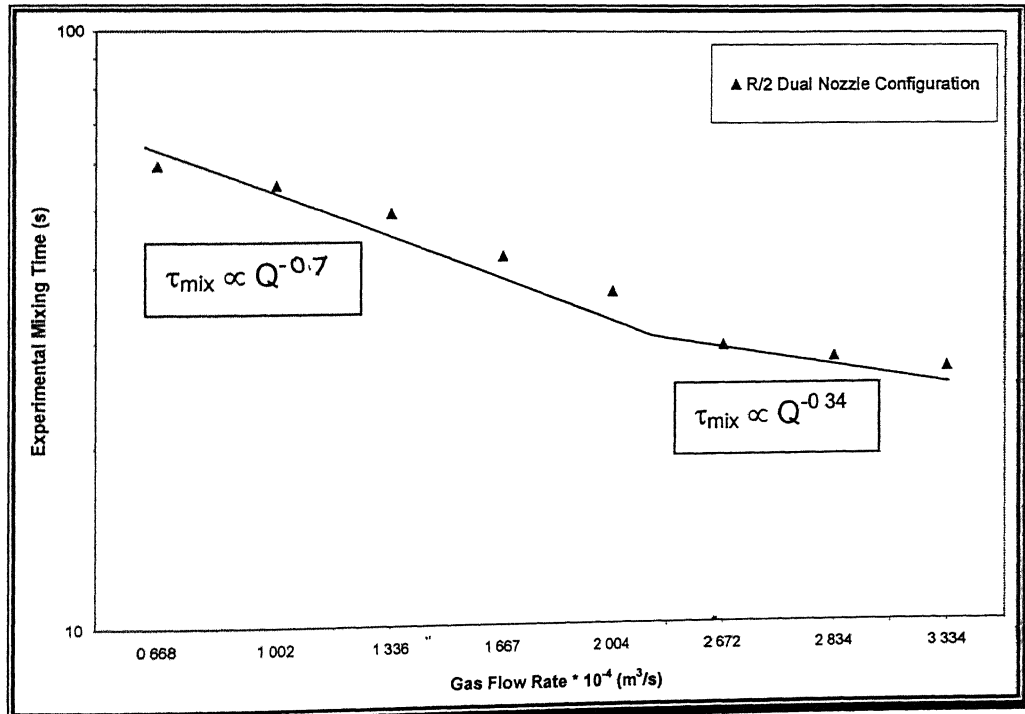
3.6   SCALING OF RESULTS

For the dual plug system with nozzles located at diametrically opposite R/2 position, the correlation derived already and presented earlier in Section 3.2 takes the following form (Recall Equation (3.6)):

$$\tau_{mix,\,95\%} = 23.4\,Q^{-0.28}\,L^{-0.52}\,R^{1.72}$$

Considering that in geometrically and dynamically similar systems gas flow rates are related according to $Q_m = \lambda^{5/2} Q_{f.s.}$, one can readily derive the ratio of mixing times between such systems from the preceding relationship. Introducing $L_m/L_{f.s.} = R_m/R_{f.s.} = \lambda$, one obtains from the above correlation

$$\left(\frac{\tau_{mix,m}}{\tau_{mix,f.s.}}\right) = \left(\frac{Q_m}{Q_{f.s.}}\right)^{-0.28} \left(\frac{L_m}{L_{f.s.}}\right)^{-0.52} \left(\frac{R_m}{R_{f.s.}}\right)^{1.72}$$

or $\quad\left(\dfrac{\tau_{mix,m}}{\tau_{mix,f.s.}}\right) = \lambda^{0.5}$ $\hspace{4cm}$ (3.10)

This is in accordance with the governing differential equation of fluid flow and mixing [37]. Similar conclusion can be drawn from the correlation proposed for R/3 nozzle configuration.

3.7   INDUSTRIAL PREDICTION

To assess the derived correlation described above in Section 3.2 for diametrically opposite R/2 dual nozzle configuration in industrial ladles, comparison of predicted mixing times as a function of specific gas flow rate (in $m^3/min.ton$) has been carried out for two industrial ladles of 150 and 500 tonne respectively at 1.0 L/D ratio. Figure 3.7 shows that

mixing times in case of 150 tonne ladles are shorter than that of the corresponding mixing times in 500 tonne ladle. Generally, diameter of a ladle increases with increase in capacity of the ladle. Also in case of a higher capacity ladle the liquid depth is more than that of a lower capacity ladle for same L/D ratio. Now, from the correlation derived for diametrically opposite R/2 dual nozzle configuration one can say that as liquid depth increases the mixing time decreases while reverse is true for vessel radius i.e. with increase in vessel radius the mixing time also increases. But the effect of vessel radius on mixing time is more pronounced than that of liquid depth according to the following:

$$\tau_{mix,\,95\%} = 23.4\,Q^{-0.28}\,L^{-0.52}\,R^{1.72}$$

$$= 23.4\,(Q_{sp}/\text{Mass of Molten Steel})^{-0.28}\,L^{-0.52}\,R^{1.72}$$

$$= 23.4\,(Q_{sp}\,/\,\rho_{Steel} \times \pi.R^2.L)^{-0.28}\,L^{-0.52}\,R^{1.72}$$

$$= 23.4 \times (\rho_{Steel} \times \pi)^{0.28} \times Q_{sp}^{-0.28} \times L^{-0.52}.L^{0.28} \times R^{1.72}.(R^2)^{0.28}$$

or, $\quad \tau_{mix,\,95\%} = 384.6\,Q_{sp}^{-0.28}\,L^{-0.24}\,R^{2.28}$ (3.11)

where, Q_{sp} is the specific industrial gas flow rate, in $m^3/s.kg$

and $\quad \rho_{Steel}$ is the density of molten steel ($= 7000\ kg/m^3$)

As the effect of vessel radius on mixing time is more pronounced than that of liquid depth, the mixing times are on the higher side for larger capacity vessels. So, we can conclude that better mixing is achieved in lower capacity ladle than that for a higher one, which truly reflects the industrial condition.

Table 3.12 presents the predicted mixing times calculated from our derived correlation in case of two industrial ladles of 150 and 500 tonne for various gas flow rates at L/D ratio 1.

74

Table 3.12: Comparison of Predicted Mixing Times for Diametrically Opposite R/2 Dual Plug Configuration for a set of Specific Gas Flow Rate in Two Industrial Ladle of 150 tonne (Diameter = 3.0m) and 500 tonne (Diameter = 4.5m).

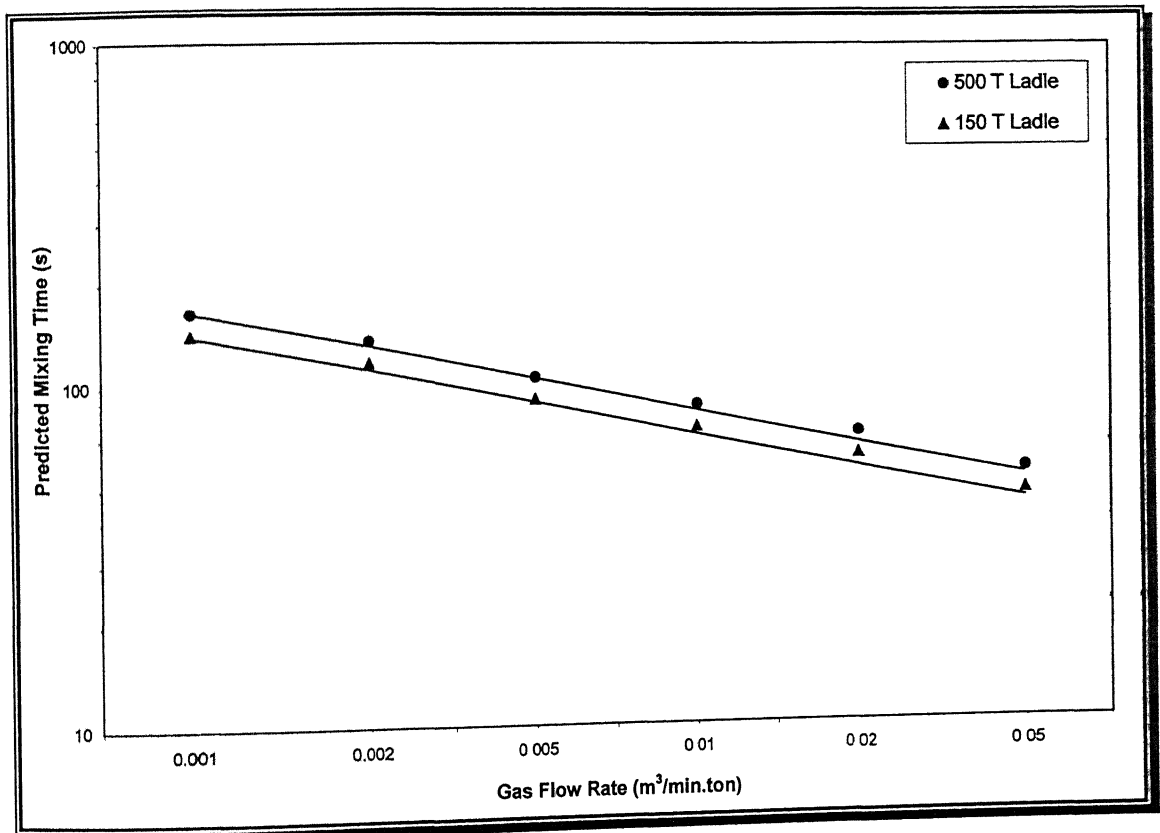| L/D Ratio	Specific Gas Flow Rate (m³/min.ton)	Predicted Mixing Time (s) $[\tau_{mix, 95\%} = 23.4\, Q^{-0.28}\, L^{-0.52}\, R^{1.72}]$	
		150 tonne Ladle	500 tonne Ladle
	0.001	142.1	165.0
	0.002	117.0	135.9
1.0	0.005	90.5	105.1
	0.010	74.6	86.6
	0.020	61.4	71.3
	0.050	47.5	55.2

Figure 3.7: Predicted mixing times as a function of gas flow rates (referenced to ladle temperature e.g. 1600°C and mean height) in different size ladles.

75

CHAPTER 4

CONCLUSIONS

Mixing times in three different cylindrical water model ladles of scale factor of 0.16, 0.13 and 0.08 of a full scale 150 tonne ladle along with a tapered 0.194 scale water model ladle (Base Diameter = 0.52m, Angle of Taper = 2.34°) were investigated experimentally over a wide range of operating conditions (nozzle(s) location, liquid depth, vessel radius and the ambient gas flow rate). From the present study following general conclusion can be drawn:

i) In the inertial force dominated flow regime, for identical net gas flow rates, mixing times in ladles agitated by twin porous plugs are shorter than those for ladles stirred with a centrally placed tuyere.

ii) The mixing times are not much sensitive to the location of twin porous plugs and it was found mixing times are practically very similar for plugs located diametrically opposite at R/3 and R/2 positions.

iii) Mixing times for twin porous plugs can be described via the following empirical correlations:

$$\tau_{mix, 95\%} = 23.9\, Q^{-0.27} L^{-0.47} R^{1.65} \qquad \text{for plugs located at R/3 positions}$$

$$\tau_{mix, 95\%} = 23.4\, Q^{-0.28} L^{-0.52} R^{1.72} \qquad \text{for plugs located at R/2 positions}$$

iv) The correlation presented above can describe mixing times in tapered vessels with reasonable amount of certainty.

v) There exists a critical gas flow rate above which the dual nozzle configurations are much more effective over a single axisymmetric nozzle configuration. And below that critical flow rate the reverse holds true.

CHAPTER 5

RECOMMENDATIONS FOR FUTURE WORK

The scope of the present work can be further expanded considering the following:

i) Mixing experiments were also carried out in a tapered vessel with diametrically opposite dual nozzle configuration. The mixing time in this case was still smaller than the mixing times for cylindrical vessel. So further studies in tapered vessel is recommended to find out advantages of vessel tapering over cylindrical one.

ii) In this present study mixing time measurements were carried out without using any viscous fluid as slag layer. Therefore, it is recommended to use some viscous oil corresponding to the viscosity of actual slag in industrial ladle to study the effect of presence of slag layer on mixing time.

BIBLIOGRAPHY

1. R. J. Fruehan : *Ladle Metallurgy Principles and Practices*, The Iron and Steel Society, Book Crafters, Inc., Chelsea, MI, 1989.

2. D. Mazumdar and R. I. L. Guthrie : *ISIJ Int.*, 1995, Vol. 35, No. 1, pp. 1-20.

3. S. H. Kim, R. J. Fruehan and R. I. L. Guthrie : *Steelmaking Proc., ISS-AIME*, Pittsburgh, PA, 1987, pp. 107-118.

4. S. H. Kim and R. J. Fruehan : *Metall. Trans. B*, 1987, Vol. 18B, pp. 381-390.

5. R. I. L. Guthrie : *Iron & Steelmaker*, Jan. 1982

6. V. Kudrin : *Steel Making*, Mir Publisers, Moscow

7. K. Mandal : *M.Tech. Thesis*, Department of Materials and Metallurgical Engineering, IIT Kanpur, Kanpur, India, 1998.

8. G. G. Krishna Murthy, S. P. Mehrotra and A. Ghosh : *Metall. Trans. B*, 1988, Vol. 19B, pp. 839-850.

9. R. W. MacDonald and L. P. Edger : *Chem. Engg. Prog.*, 1951, Vol. 47, pp. 363-369.

10. R. Baker, A. S. Normanton, G. D. Spenceley and R. Atkinson : *Ironmaking and Steelmaking*, 1980, Vol. 7, pp. 227-238.

11. R. Henrion : *Ironmaking and Steelmaking*, 1980, Vol. 7, pp. 239-241.

12. M. Saigusa, J. Nagai, F. Sudo, H. Bada and S. Yamada : *Ironmaking and Steelmaking*, 1980, Vol. 7, pp. 242-248.

13. Y. Sahai and R. I. L. Guthrie : *Advances in Transport Processes*, 1986, Vol. 4, pp. 1.

14. D. Mazumdar : *Ph.D. Thesis*, Department of Mining and Metallurgical Engineering, McGill University, Montreal, PQ, Canada, 1985.

15. J.B. Gray : *Chem. Engg. Prog.*, 1963, Vol. 59, pp. 55-59.

16. C. J. Hoogendoorn and A. P. Denttartog : *Chem. Engg. Sci.*, 1967, Vol. 22, pp. 1689-1699.

17. S. C. Koria and K. W. Lange : *Arch. Eisenhuttenwes.*, 1984, Vol. 55, pp. 97-100.

18. J. Y. Oldshue, H. E. Hirschland A. T. Gretton : *Chem. Engg. Prog.*, 1956, Vol. 52, pp. 481-484.

19. J. G. Vande Vusse : *Chem. Engg. Sci.*, 1955, Vol. 4, pp. 178-200.

20. K. Nakanishi, T. Fujii and J. Szekely : *Ironmaking and Steelmaking*, 1975, Vol. 2, pp. 193-197.

21. U. P. Sinha and M. J. McNallan : *Metall. Trans. B*, 1985, Vol. 16B, pp. 850-853.

22. H. Kramers, G. M. Barrs and W. H. Knoll : *Chem. Engg. Sci.*, 1953, Vol. 2, pp. 35-42.

23. S. Asai, T. Okamoto, J. He, and I. Muchi : *Trans. ISIJ*, 1983, Vol. 23, pp. 43-50.

24. Y. Sahai and R. I. L. Guthrie : *Metall.Trans. B*, 1982, Vol. 13B, pp. 125-127.

25. Y. Sahai and R. I. L. Guthrie : *Metall.Trans. B*, 1982, Vol. 13B, pp. 203-211.

26. D. Mazumdar and R. I. L. Guthrie : *Metall.Trans. B*, 1985, Vol. 16B, pp. 83-90.

27. M. Y. Zhu, T. Inomoto, I. Sawada and T. C. Hsiao : *ISIJ Int.*, 1995, Vol. 35, No. 5, pp. 472-479.

28. S. Joo and R. I. L. Guthrie : *Metall. Trans. B*, 1992, Vol. 23B, pp. 765-778.

29. J. Meitz and F. Oeters : Steel Res., 1988, Vol. 59, pp. 52.

30. J. Meitz and F. Oeters : Steel Res., 1989, Vol. 60, pp. 387-394.

31. D. Mazumdar and R. I. L. Guthrie : *Metall. Trans. B*, 1986, Vol. 17B, pp. 725-733.

32. D. Mazumdar : A proposal submitted to the Ministry of Steel and Mines on *"Mixing and Mass Transfer in Steelmaking Ladles stirred with Dual Porous Plug : A Physical and Mathematical Model Investigation."*

33. D. Mazumdar and R. I. L. Guthrie : *ISS Transactions*, September 1999, pp. 89-96.

34. A. Ghosh and D. Mazumdar : *A Short-Term Course on Secondary Steel Making*, Department of Materials and Metallurgical Engineering, IIT Kanpur, Kanpur, India.

35. A. Ghosh : *Secondary Steelmaking - Principles and Applications*, CRC Press.

36. *IIIrd Quarterly Project Report* (March, 2002 to May, 2002) : Department of Materials and Metallurgical Engineering, IIT Kanpur, Kanpur, India, May, 2002.

37. D. Mazumdar, H. B. Kim and R. I. L. Guthrie *: Ironmaking and Steelmaking*, 2000, Vol. 27, pp. 302-309.

38. *IVth Quarterly Project Report* (June, 2002 to August, 2002) : Department of Materials and Metallurgical Engineering, IIT Kanpur, Kanpur, India, August, 2002.

39. *V^{th} Quarterly Project Report* (September, 2002 to November, 2002) : Department of Materials and Metallurgical Engineering, IIT Kanpur, Kanpur, India, November, 2002.

40. http:// davidmlane.com/hyperstat

41. *Supreme Pocket Master – Maths Formulae*, Kalra Publication Pvt. Ltd., Delhi, pp. 180.

APPENDIX

Correlation Coefficient

A correlation coefficient is a number between -1 and 1 which measures the degree to which two variables are linearly related. If there is perfect linear relationship with positive slope between the two variables, we have a correlation coefficient of 1; if there is positive correlation, whenever one variable has a high (low) value, so does the other. If there is a perfect linear relationship with negative slope between the two variables, we have a correlation coefficient of -1; if there is negative correlation, whenever one variable has a high (low) value; the other has a low (high) value. A correlation coefficient of 0 means that there is no linear relationship between the variables

Multiple Regression Correlation Coefficient

The multiple regression correlation coefficient, R^2, is a measure of the proportion of variability explained by, or due to the regression (linear relationship) in a sample of paired data. It is a number between zero and one and a value close to zero suggests a poor model.

A very high value of R^2 can arise even though the relationship between the two variables is non-linear. The fit of a model should never simply be judged from the R^2 value.

Root-Mean-Square (rms) Deviation

Root-mean-square (rms) deviation: A single quantity, σ_{rms}, characterizing a function, $f(x)$, given by,

$$\sigma_{rms} = \sqrt{\frac{1}{M_0}\int_{-\infty}^{\infty}(x - M_1)^2 f(x)\, dx} \quad , \quad \text{where}$$

$$M_0 = \int_{-\infty}^{\infty} f(x)\, dx \quad , \quad \text{and}$$

$$M_1 = \frac{1}{M_0}\int_{-\infty}^{\infty} x\, f(x)\, dx$$

Just like the correlation coefficients, the root-mean-square (rms) deviation is an indicator recommended to be used for comparing various models representing the same dependent variable. A model with smaller root-mean-square (rms) represents the data more accurately than a model with larger values of the indicator.

Variance

The variance is a measure of how spread out a distribution is. It is computed as the average squared deviation of each number from its mean. For example, for the numbers 1, 2, and 3, the mean is 2 and the variance is:

$$\sigma^2 = [(1\text{-}2)^2 + (2\text{-}2)^2 + (3\text{-}2)^2]\,/\,3 = 6.67$$

the formula (in simulation notation) for the variance in a population is:

$$\sigma^2 = \frac{\Sigma(X - \mu)^2}{N}$$

where μ is the mean and N is the number of scores.

When the variance is computed in a sample the statistic,

$$s^2 = \frac{\Sigma(X - M)^2}{N}$$

(where M is the mean of the sample) can be used. S^2 is a biased estimate of σ^2, however. By far the most common formula for computing variance in a sample is:

$$s^2 = \frac{\Sigma(X - M)^2}{N-1}$$

which gives an unbiased estimate of σ^2. Since samples are usually used to estimate parameters, s^2 is the most commonly used measure of variance.

Just like root-mean-square deviation, a model with smaller variance represents the data more accurately than a model with larger values of variance.

A 145116